Bandstructure Observation of Graphene Nanoribbon and Boron-Nitride Nanoribbon Embedded Graphene Nanoribbon

A Thesis Submitted
For the partial contentment for the Degree of
Bachelor of Science in Electrical and Electronic Engineering to the
Department of Electrical and Electronic Engineering
BRAC University
Dhaka-1212, Bangladesh

By

Fatin Farhan Haque-12321043

Rimi Reza Duity-12121091

Syed Shamsia Tanzin Authoi-12321035

April 2016

Candidate Declaration

We hereby declare that the thesis titled "Bandstructure observation of Graphene Nanoribbon and Boron-Nitride embedded Graphene Nanoribbon" is submitted to the Department of Electrical and Electronic Engineering of BRAC University with the aim of completion for the degree of Bachelor of Science in Electrical and Electronic Engineering. The following work is our original productuion and has not submitted elsewhere for the award of any other degree, diploma or any kind of publication.

Date: 19th April 2016

Dr. Md. Belal Hossain Bhuian
Thesis Supervisor

_____

Atanu Kumar Saha
Thesis Co-Supervisor

_____

Authors:

Fatin Farhan Haque
Student ID: 12321043

_____

Rimi Reza Duity
Student ID: 12121091

_____

Syed Shamsia Tanzin Authoi
Student ID: 12321035

_____

Acknowledgement

Firstly, we would like to express our gratitude to our respected thesis supervisor, Dr. Mohammed Belal Hossain Bhuian, Associate Professor, Department of Electrical and Electronic Engineering (EEE), BRAC University; for his supportive supervision and feedbacks during the completion of the thesis. Secondly, our gratitude is towards our thesis co-supervisor, Atanu Kumar Saha, Lecturer, Department of Electrical and Electronic Engineering (EEE), BRAC University; for enabling us to develop the core concepts and guiding us throughout patiently. Next we would like to attribute our thankfulness towards BRAC University for providing us with resources required for the research, and every other individual without whose contribution, the research would not be a success.

Abstract

Due to distinctive electronic properties and potential future application in tunable bandgap opening, Graphene Nanoribbon (GNR) has apprehended strong attention. Boron Nitride Nanoribbons (BNNR) exhibit analogous structure. Thus domains of Graphene embedded in Boron Nitride can be synthesized to open a bandgap exposing the semiconductor behavior of Graphene more precisely. A numeric investigation of the impact of GNR embedded in BNNR explains the bandgap tunability as well as transport property of Graphene. This unique versatility is likely to bring a radical change in electrical field not only by encouraging innovation but also by improving the mechanism of existing devices.

Table of Contents

List of Figures

List of Tables

Abbreviation

BN: Boron Nitride

h-BN: hexagonal Boron Nitride

GNR: Graphene Nano Ribbon

BNNR: Boron Nitride Nano Ribbon

AGNR: Armchair Graphene Nano Ribbon

ZGNR: Zigzag Graphene Nano Ribbon

ABNNR: Armchair Boron Nitride Nano Ribbon

ZBNNR: Zigzag Boron Nitride Nano Ribbon

DFT: Density Functional Theory

TB: Tight Binding

DOS: Density of States

HOMO: Highest Occupied Molecular Orbital

LUMO: Lowest Unoccupied Molecular Orbital

GUI: Graphical User Interface

Chapter 1: Introduction

Graphene, a two-dimensional single-atom thick membrane of carbon atoms arranged in a honeycomb crystal, has been the most widespread material due to its excellent electrical, magnetic, thermal, optical and mechanical properties. Bilayer graphene is also an important material as it has very unique electronic structure as well as transport properties. On the other hand, Boron Nitride, a hexagonal lattice consisting of analogous structure as graphene has recently attracted much attention due to its superior mechanical and thermal conducting properties. Though both were discovered in the same century the difficulties of different production techniques and high cost of BN has limited its fabrication practices for about hundred years. In contrast to the zero bandgap of graphene, BN Nano Ribbons exhibit a wide bandgap suitable for semiconductors, optoelectronics and dielectric substrate for high-performance graphene electronics. Graphene sandwiched by monolayer BN is predicted to have a tunable bandgap without sacrificing its mobility.

(a) (b)

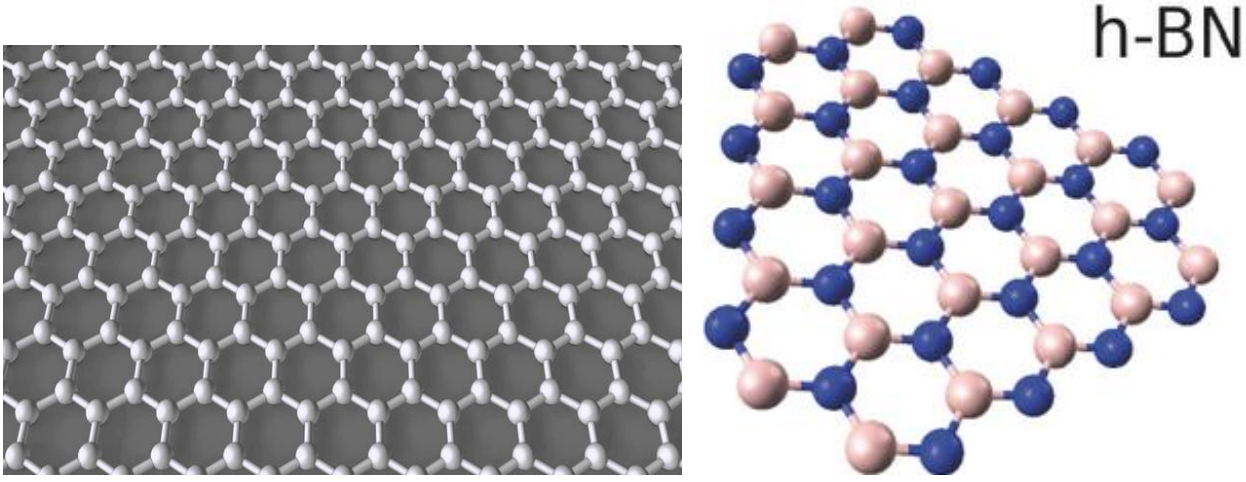

Fig. 1: (a) Atomic Structure of Graphene (b) Atomic Structure of Boron Nitride. [1]

1.1 Lattice Structure and orbital hybridization of Graphene and BN:

Both Graphene and Boron Nitride are defined by sp^2 hybridization. sp^2 hybridized orbital is responsible for bonding in p_x and p_y orbital of graphene and remaining p_z orbital is situated perpendicularly to that plane. This perpendicular orbital contributes one conducting electron for per carbon atom. Thus among these four valence orbitals $(2s, 2p_x, 2p_y, 2p_z)$ of carbon atom the s, p_x, p_y orbitals combine to form the in-plane occupied orbital (σ) and unoccupied orbital(σ^*). These orbitals are even planner symmetry. The p_z orbital which is an odd planner symmetry forms localized π and π^* orbital. The bonding orbitals are strongly covalent bonds determining the energetic stability and the elastic properties of Graphene. The remaining $p_z$orbital is odd with respect to the planner symmetry and decoupled from the bonding states. From the lateral interaction with neighboring $p_z$orbitals, localized π and π^* orbitals are formed. Graphite consists of a stack of many Graphene layers. The unit cell in Graphene can be primarily defined using two graphene layers translated from each other by a C-C distance, $a_{c-c} = 1.42\text{Å}$. The three-dimensional structure of Graphite is maintained by weak interlayer Van Der Waals interaction between π bond so adjacent layers, which generate a weak but finite out-of-plane delocalization.

(a) (b)

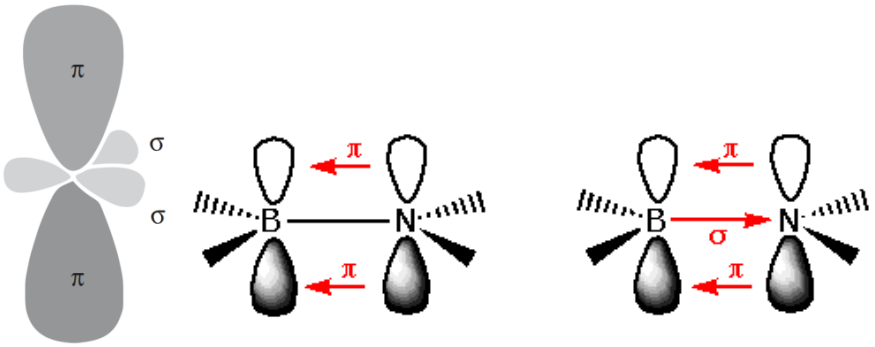

Fig. 1.1: (a) sp^2 Hybridization of Graphene, (b) sp^2 Hybridization of BN. [2]

Boron having electronic structure of $1s^2 2s^2 2p^1$along with nitrogen with an electronic structure of $1s^2 2s^2 2p^3$, forms sp^2 hybrid bonds in the B-N sheets. In sp^2 hybridization Boron uses all of the outer electrons to give the configuration $1s^1 2p_x^1 2p_y^1 2p_z^2$ when fabricated with Nitrogen. After formation of the sp^2 orbital, the remaining two p electrons are located in the (filled) p_z orbital. The σ bonding in the BN sheets that result is strong and similar to the bonding in the graphite sheets. However, π bonding between the full $2p_z$orbitals of nitrogen and the empty $2p_z$ orbitals of boron is not possible. This is because the orbital energies of boron and nitrogen are too dissimilar for a large energy gain. Thus no delocalized electron is present in the structure. Because of this the boron and nitrogen atoms in alternate layers avoid each other. This allows for the more efficient packing of the filled p_z orbitals, and the layers are closer than they are in graphite. Nevertheless, the lack of bonding between the layers still means that BN retains the easy cleavage of graphite and still is a good dry lubricant.

1.2 Motivation and Objective of the work:

At present the biggest challenges in fabricating effective nano scale devices are speed limitation and excessive power consumption. Using Graphene in such devices high mobility can be obtained but due to the high on current and high off current, the on off current ratio of Graphene becomes low. Thus the material exhibits no bandgap and tunneling effect occurs. On the other hand, BN has efficiently high band gap due to high on-off current ratio but has low mobility. When embedded in Nanoribbon forms the off current of Graphene can significantly be reduced to make the on-off current ration high enough for suitable bandgaps for any ribbon width index and also preserve the high mobility of Graphene. Thus, the possibility of opening a tunable bandgap in graphene by confining it within BN has been the motivation as well as the objective of the paper.

1.3 Framework of Research:

Firstly, the energy dispersion relation has of both Graphene and BN been determined using first nearest TB model and evaluated using the General Schrodinger equation. Afterwards their bandgaps, hierarchy and DFT evaluated Tight Binding parameters have been examined and listed. Afterwards using those parameters the band structure of Graphene Nanoribbons as well as Boron Nitride Nanoribbons has been observed. Finally, Graphene Nanoribbons embedded in BN Nanoribbons have been fabricated to attain the objective of the work. A GUI has also been developed that shows direct comparison between GNR and BNNR embedded GNR along with corresponding ribbons.

Chapter 2: Energy Dispersion Relation of Graphene and Boron Nitride

Graphene, a single atomic sheet of periodically arranged graphite forming an infinite honeycomb lattice, is a two-dimensional allotrope having a single layer of sp^2 - bonded carbon atoms that are densely packed. Ever since the first demonstration of its zero bandgap, the lattice has attracted much attention not only for its exceptional strength and thermal conductivity but also for electrical conductivity. Since Carbon (C), Boron (B) and Nitrogen (N) are all in the same period of the periodic table, single layer hexagonal Boron Nitride (h-BN) exhibits analogous honeycomb structure as Graphene and also has distinct bandgap variation trends. Moreover, the band structure and energy dispersion relation of Graphene and BN provides better understanding in analyzing the possibilities of opening a tunable bandgap when Graphene Nano Ribbons (GNR) are embedded in BN Nano Ribbons (BNNR). Among all possible band structure calculation methodologies Density Functional Theory (DFT) and nearest Tight Binding (TB) method have been employed in this paper in order to find appropriate bandgap. [11-14]

2.1 Introduction to DFT (Density Functional Theory):

Since 1970s Density functional theory (DFT) has been considered the most versatile method for quantum mechanical calculation. However it did not get complete recognition until the year of 1990s. In the following year the approximations used in theory was redefined to such an extent that they satisfactorily agreed with the experimental data, especially the ones attained from first principles calculation. Hence, DFT has been defined as the quantum mechanical modelling method used to investigate the electronic band structure as well as other electronic properties of atoms, molecules and condensed phases. Using this theory, the

properties of a many-electron system can be evaluated specially the ones dependent on electron density. The name Density Functional Theory has been driven from the fact that DFT incorporates the use of functionals of the electron density. Compared to costly methods like first principles calculation or Hartree-Fock theory DFT is much cost-effective. [24]

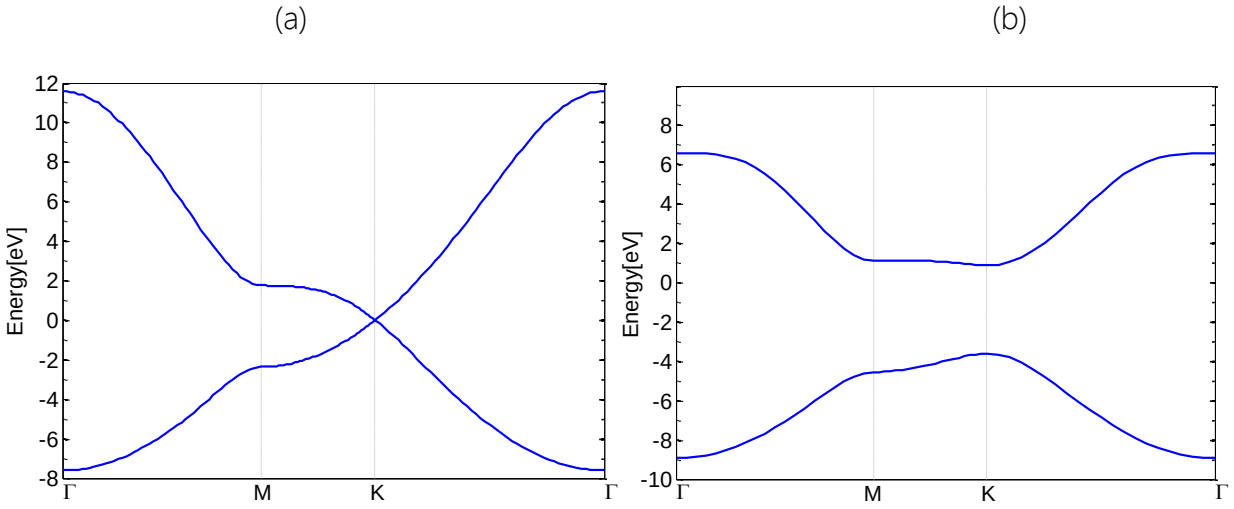

Fig 2.1: (a) Band Structure of Graphene using DFT calculation. (b) Band Structure of BN using DFT calculation.

2.2 Introduction to nearest neighbor TB (Tight Binding) model:

Tight-binding models are applied to a wide variety of matters and they give good qualitative results in many cases. The nearest TB model is defined as an approach that calculates electronic band structures using an approximate set of wave functions based on superposition of wave functions for isolated atoms located at each atomic site. It is closely related to the Linear Combination of Atomic Orbitals method (LCAO).TB overlap as well as Hamiltonian matrices directly from first-principles calculations has always been a subject of continuous interest. Since, the nearest TB model primarily attempts to represent the electronic structure of condensed matter using a minimal atomic-orbital like basis set; it has been redefined to fit the resultants of first-principles calculations.

Usually, first-principles calculations are done using a large or long-ranged basis set in order to get convergent results, while tight-binding overlap and Hamiltonian matrices are based on a short-ranged minimal basis representation. Therefore in this paper, we performed a transformation that can carry the electronic Hamiltonian matrix from a large or long-ranged basis representation onto a short ranged minimal basis representation in order to obtain an accurate tight-binding Hamiltonian from first principles calculation. [3]

2.3 Band Structure (E-k relation) calculation:

Electronic band structure of a matter is described by the ranges of energy that an electron within the matter may have and also the ranges of energy that it may not have (called band gaps or forbidden bands). By examining the allowed quantum mechanical wave functions for an electron in a large, periodic lattice of atoms or molecules, the electronic bands and band gaps can effectively be derived. Again by knowing the band structures of Graphene and 2D h-BN lattice, their future possibilities in making better Nano-scaled devices can easily be comprehended. Since ab-initio DFT method effectively represents first principles calculation, the parameters of nearest TB model have been modified to follow the variation trends of DFT calculation. Therefore, for electronic band gap calculation DFT and Nearest TB model have been employed in this paper.

From First principles calculations it has been observed that the electronic bands near the Fermi level are contributed from the π orbitals of the atoms. Thus a π -orbital nearest TB model has been engaged to investigate quantum confinement as well as edge effects on the electronic band structure of both Graphene and BN. Compared to the time consuming First principles calculation, this modified nearest TB method can be effectively applied to study

more intricate low dimensional Nano structures whose properties are controlled by π electrons.

To attain the π -orbital nearest TB Hamiltonian and derive the electronic spectrum of the total Hamiltonian, the corresponding Schrodinger equation has to be solved. According to time-independent Schrodinger's equation: [3, 5-7]

$$E(\vec{K})\psi(\vec{K},\vec{r}) = \hat{H}\psi(\vec{K},\vec{r}) \qquad (2.1)$$

Where,

$\hat{H}$=H_{op}=Hamiltonian operator

E= Eigen Energy (expectation value of the orbital energy)

ψ = Eigen function (molecular orbital wave function)

Because of translational symmetry in a particular lattice the molecular Eigen functions can be written as the linear combination of atomic Eigen functions ψ_j $(j = 1,2,3\ldots\ldots,n)$; where n is the number of Bloch wave functions) and Bloch orbital (appendix) basis functions $a_j(\vec{r})$:

$$\psi_M = \sum_{j=1}^{n} \psi_j \, a_j$$

However, this Linear Combination of Atomic Orbital (LCAO) gives approximate solution instead of exact solution of the Schrodinger's equation. Thus we incorporated the Variational principal where, for a particular wave function, the expected value of orbital energy or Eigen energy is given by:

$$E = \frac{\int \psi^* \hat{H} \, \psi \, dr}{\int \psi^* \psi \, dr} \qquad (2.2)$$

The following principle also states that the value of E obtained by using equation (2.1) is always greater than that of the exact solution.

General form of equation:

$$E\psi_n = \sum_m H_{nm}\psi_m \qquad (2.3)$$

For both 2D and 3D lattice:

$\psi_n = \psi_0 e^{\vec{k}.\vec{r}_n}$; where $\vec{r}_n$ is the position (position vector) of the n^{th} atom.

To calculate $E(k)$ relation for 2D or 3D lattice the following equation is formed:

$$E\psi_0 e^{i\vec{k}\vec{r}_n} = \sum_m H_{mn}\psi_0 e^{i\vec{k}.\vec{r}_m}$$

$$E\psi_0 = \sum_m H_{mn}\psi_0 e^{i\vec{k}.(\vec{r}_m - \vec{r}_n)}$$

$$E = \sum_m H_{mn} e^{i\vec{k}.(\vec{r}_m - \vec{r}_n)}$$

$$E(\vec{k}) = \sum_m H_{mn} e^{i\vec{k}.(\vec{r}_m - \vec{r}_n)} \qquad (2.4)$$

Here, $(\vec{r}_m - \vec{r}_n)$ is the vector that runs from m^{th} atom to n^{th} atom.

Self-integrals can be defined as, $\varepsilon = \langle\psi_n|\hat{H}|\psi_n\rangle$

Hopping integrals can be defined as, $t = \langle\psi_{n-1}|\hat{H}|\psi_n\rangle$ *or* $\langle\psi_n|\hat{H}|\psi_{n+1}\rangle$

2.3.1 Energy Dispersion (E-k relation) calculation of Graphene:

Carbon atoms in a Graphene plane are located at the vertices of a hexagonal lattice where each C atom is surrounded by three C atoms. The following Graphene network in Fig.2.3.2(a) can be regarded as a triangular Bravais lattice with two atoms (A and B) per unit cell along with basis vectors $\hat{a}_1$ and $\hat{a}_2$, where

$$\hat{\boldsymbol{a}}_1 = \frac{\sqrt{3}}{2}\hat{\boldsymbol{a}}_x + \frac{1}{2}\hat{\boldsymbol{a}}_y \text{ (First primitive vector)}$$

$$\hat{\boldsymbol{a}}_2 = \frac{\sqrt{3}}{2}\hat{\boldsymbol{a}}_x - \frac{1}{2}\hat{\boldsymbol{a}}_y \text{ (Second primitive vector)}$$

(a) (b)

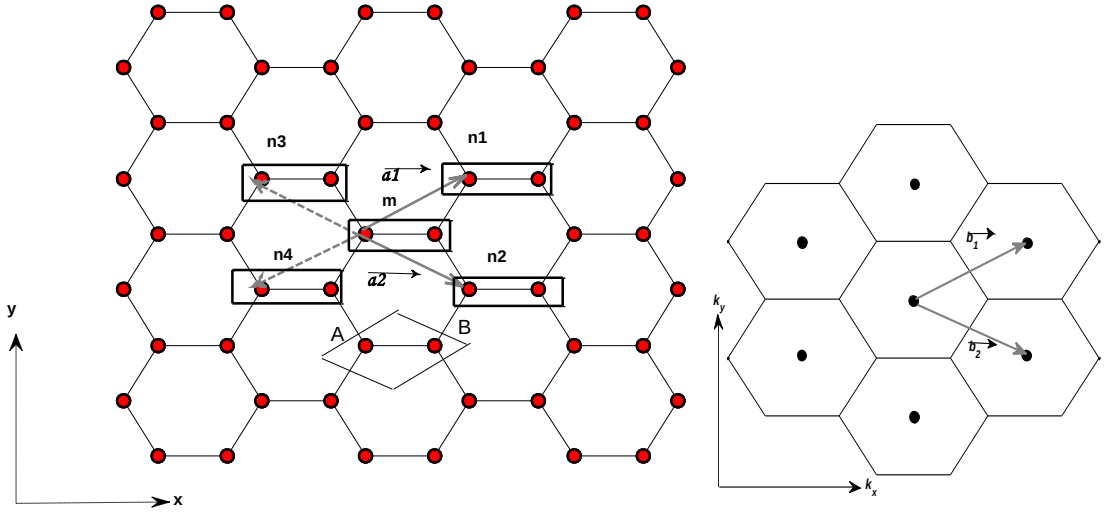

Fig. 2.3.1: (a) Real Space Lattice of Graphene, (b) Reciprocal Space Lattice of Graphene.

Here, $\boldsymbol{a} = \sqrt{\boldsymbol{3}}\boldsymbol{a}_{\boldsymbol{C-C}}$,where $\boldsymbol{a}_{\boldsymbol{C-C}} = \boldsymbol{1.42}$Å is the carbon-carbon distance in graphene. From the figure we can see that each A or B-type atom is surrounded by three opposite type.

By using condition $a_i . b_j = 2\pi\delta_{ij}$, the reciprocal lattice vectors ($\hat{b}_1$ and $\hat{b}_2$) can be obtained where,

$$\hat{b}_1 = b(\frac{1}{2}\hat{k}_x + \frac{\sqrt{3}}{2}\hat{k}_y)$$

$$\hat{b}_2 = b(\frac{1}{2}\hat{k}_x - \frac{\sqrt{3}}{2}\hat{k}_y)$$

Where, $b = \frac{4}{3a(c-c)} = \frac{4}{a\sqrt{3}}$. These vectors are shown in Fig. 2.3.2(b) together with the first Brillouin zone. The hexagonal shaped Brillouin zone is built as the Wigner-Seitz cell of reciprocal lattice. Out of its six corners, two of them are equivalent (the others can be written as one of these two plus a reciprocal lattice vector). These two special points are denoted with K_+ and K_-. Another high symmetry point is the one labeled with M in the Fig. 2.3.2(b).

When carbon atoms are placed onto the Graphene hexagonal network Fig. 2.3.2 (a), the electronic wavefunctions from different atoms overlap. However, because of symmetry the overlap between the $p_z$orbitals and the s or the $p_x$and $p_y$electrons are strictly zero. Therefore, the $p_z$electrons which form the π bonds in Graphene can be treated independently from other valence electrons. Within this π-band approximation, the A-atom or B-atom is uniquely defined by one orbital per atom site $p_z(\vec{r}-\vec{r}_A)$ or $p_z(\vec{r}-\vec{r}_B)$.

According to Bloch's theorem, the Eigen-functions evaluated at two given Bravais lattice points $\vec{r}_m$and $\vec{r}_n$ differ from each other in just a phase factor, $e^{(i\vec{k}(\vec{r}_m-\vec{r}_n))}$.Using the orthogonality relation in the Schrodinger equation, $H\psi = E\psi$, the energy dispersion relation can be easily obtained from the diagonalization of $E(\vec{K})$.

For calculating the dispersion relation of Graphene lattice two C-C molecules m and n_1 (as shown in the Fig.2.3.1a) are considered first. $E(k_x, k_y)$ or E is considered to be the energy of the system depending on the k vector.

Since from secular equation it has been obtained that ε are the Site energies of Carbon, thus

C-C self-interaction (for A type-A type or B type-B type) = ε

And (A type-B type) hopping integral = t

In matrix form the diagonal elements become: $\begin{bmatrix} \varepsilon & t \\ t & \varepsilon \end{bmatrix}$

Similarly, the interactions $(m-n1\,),(m-n2)$ form upper diagonal matrix $\begin{bmatrix} 0 & 0 \\ t & 0 \end{bmatrix}$ and $(m-n3),(m-n4)$ form lower diagonal matrix $\begin{bmatrix} 0 & t \\ 0 & 0 \end{bmatrix}$. Therefore taking $\hat{\mathrm{a}}_1$ and $\hat{\mathrm{a}}_2$ into account the relation is given by:

$$E(\vec{K}) = \begin{bmatrix} 0 & t \\ 0 & 0 \end{bmatrix} e^{-i\vec{k}\hat{a}_2} + \begin{bmatrix} 0 & t \\ 0 & 0 \end{bmatrix} e^{-i\vec{k}\hat{a}_1} + \begin{bmatrix} \varepsilon & t \\ t & \varepsilon \end{bmatrix} + \begin{bmatrix} 0 & 0 \\ t & 0 \end{bmatrix} e^{i\vec{k}\hat{a}_1} + \begin{bmatrix} 0 & 0 \\ t & 0 \end{bmatrix} e^{i\vec{k}\hat{a}_2}$$

$$\begin{bmatrix} \varepsilon & t + te^{-i\vec{k}\hat{a}_1} + te^{-i\vec{k}\hat{a}_2} \\ t + te^{i\vec{k}\hat{a}_1} + te^{i\vec{k}\hat{a}_2} & \varepsilon \end{bmatrix}$$

Here,

$$E(\vec{K}) = \varepsilon \pm |h_0|, \text{ where } h_0 = t + te^{i\vec{k}\hat{a}_1} + te^{i\vec{k}\hat{a}_2}$$

$$h_0 = t(1 + e^{i\vec{k}\hat{a}_1} + e^{i\vec{k}\hat{a}_2})$$

$$h_0 = t[1 + e^{i\vec{k}(\hat{a}_x + \hat{b}_y)} + e^{i\vec{k}(\hat{a}_x - \hat{b}_y)}]$$

$$h_0 = t[1 + e^{i\vec{k}_x a + i\vec{k}_y b} + e^{i\vec{k}_x a - i\vec{k}_y b}]$$

$$h_0 = t[1 + e^{i\vec{k}_x a}\left(e^{i\vec{k}_y b} + e^{-i\vec{k}_y b}\right)]$$

$$h_0 = t[1 + \ e^{i\vec{k}_x a}\ 2\cos\vec{k}_y b]$$

$$h_0 = t[1 + \left(\cos\vec{k}_x a + i\sin\vec{k}_x a\right)2\cos\vec{k}_y b]$$

$$h_0 = t[1 + 2\cos\vec{k}_y b\cos\vec{k}_x a + 2i\cos\vec{k}_y b\sin\vec{k}_x a]$$

$$|h_0| = \sqrt{(1 + 2\cos\vec{k}_y b\cos\vec{k}_x a)^2 + (2\cos\vec{k}_y b\sin\vec{k}_x a)^2}$$

$$|h_0| = \sqrt{\left(1 + 4\cos\vec{k}_y b\cos\vec{k}_x a + 4\cos^2\vec{k}_y b\cos^2\vec{k}_x a\right) + 4\cos^2\vec{k}_y b\sin^2\vec{k}_x a}$$

$$|h_0| = \sqrt{1 + 4\cos\vec{k}_y b\cos\vec{k}_x a + 4\cos^2\vec{k}_y b(\sin^2\vec{k}_x a + \cos^2\vec{k}_x a)}$$

$$|h_0| = \sqrt{1 + 4\cos\vec{k}_y b\cos\vec{k}_x a + 4\cos^2\vec{k}_y b}$$

Now,

$$a = \frac{3}{2}a_0 \; and \; b = \frac{\sqrt{3}}{2}a_0$$

$$E(\vec{k}) = \varepsilon \pm t\sqrt{1 + 4\cos\vec{k}_y\frac{\sqrt{3}}{2}a_0\cos\vec{k}_x\frac{3}{2}a_0 + 4\cos^2\vec{k}_y\frac{\sqrt{3}}{2}a_0} \qquad (2.5)$$

Using this equation the hexagonal shaped Brillouin zone of Graphene can be obtained. The $\boldsymbol{K_+}$, $\boldsymbol{K_-}$ and $\boldsymbol{M}$ valley are shown in Fig. 2.3.3. The center is denoted as Gamma $(\boldsymbol{\Gamma})$ valley.

(a) (b)

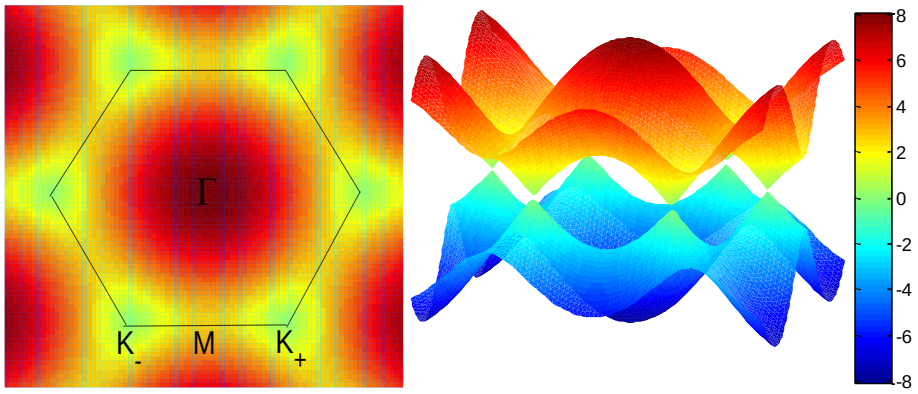

Fig 2.3.2: (a) First Brillouin zone (BZ) of graphene. (b) Energy dispersion relation of graphene.

The wave-vectors $k = (k_x, k_y)$ are chosen within the first hexagonal Brillouin zone. The zeros of h_0 (k) correspond to the crossing of the bands with the + and – signs. One can verify that $h_0(k = k_+) = h_0(k = k_-) = 0$ and therefore the crossing over occurs at the points $k_+ \; and \; k_-$. Furthermore, with a single p_z electron per atom in the $\pi - \pi *$ model (the three other s, p_x, p_yfill the low-lying σ band), the (-) band (negative energy band) is fully occupied, while the (+) band (positive energy band) is empty, at least for electrically neutral Graphene. Thus, the fermi level E_F (charge neutrality point) in the zero-energy reference in Fig.2.3.3 (b) and fermi surface is composed of the set of $k_+ \; and \; k_-$ points. Thereby, Graphene displays a metallic (zero-bandgap) character. However, as the Fermi surface is of zero dimensions (since it is reduced to a discrete and finite set of points), the term semi-metal or zero-gap semiconductor is usually employed. Expanding for kin the vicinity of $k_+ \; or \; k_-$, $k = \; k + \delta k$ or $k = \; k - \delta k$, yields a linear dispersion for the π and π* bands near these six corners of 2D hexagonal Brillouin Zone.

2.3.2 Band Structure and Energy Dispersion calculation of BN:

B and N atoms in a BN plane are located at the vertices of a hexagonal lattice where each B is surrounded by three N atoms and each N is surrounded by three B atoms. The following BN network in Fig.2.3.4can be regarded as a triangular Bravais lattice with two atoms (one B and one N) per unit cell along with basis vectors $\hat{a}_1$ and $\hat{a}_2$,where

$$\hat{\boldsymbol{a}}_1 = \frac{\sqrt{3}}{2}\hat{\boldsymbol{a}}_x + \frac{1}{2}\hat{\boldsymbol{a}}_y \text{ (First primitive vector)}$$

$$\hat{\boldsymbol{a}}_2 = \frac{\sqrt{3}}{2}\hat{\boldsymbol{a}}_x - \frac{1}{2}\hat{\boldsymbol{a}}_y \text{ (Second primitive vector)}$$

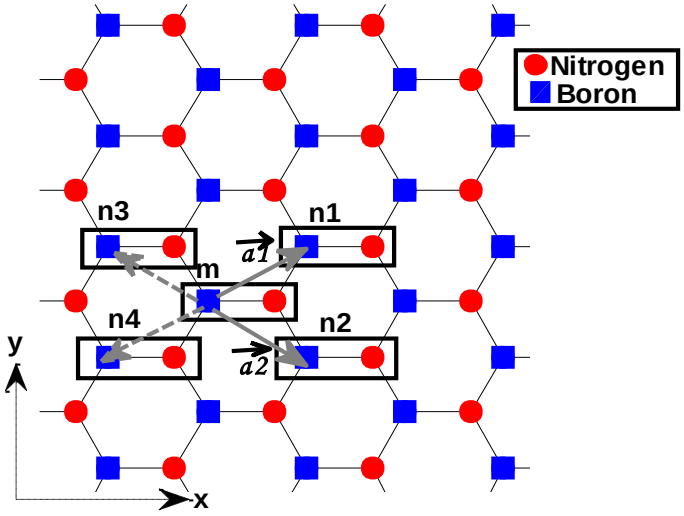

Fig. 2.3.3: Real space lattice of h-BN.

Here, $\boldsymbol{a = \sqrt{3} a_{B-N}}$, where $\boldsymbol{a_{B-N} = 2.512}$Å is the Boron-Nitrogen distance in BN. 2D h-BN exhibits similar Brillouin zone formation due to its analogous structure as Graphene. According to Bloch's theorem, the Eigen-functions evaluated at two given Bravais lattice points $\vec{\boldsymbol{r}}_{\boldsymbol{m}}$ and $\vec{\boldsymbol{r}}_{\boldsymbol{n}}$ differ from each other in just a phase factor, $\boldsymbol{e^{i\vec{k}(\vec{r}_m - \vec{r}_n)}}$.Using the orthogonality relation in the Schrodinger equation, $\boldsymbol{H\psi = E\psi}$, the energy dispersion relation can be easily obtained from the diagonalization of Energy dispersion relation.

For calculating the $\boldsymbol{E(k)}$ dispersion relation of 2D h-BN lattice two BN molecules m and n_1 (as shown in the Fig.2.3.4) are considered first. $\boldsymbol{E(k_x, k_y)}$ or $\boldsymbol{E}$ is considered to be the energy of the system depending on the k vector.

Since from secular equation it has been obtained that $\boldsymbol{\varepsilon_B}$ and $\boldsymbol{\varepsilon_N}$ are the Site energies of Boron and Nitrogen respectively,

B-B self-interaction= $\varepsilon_B - E(k_x, k_y) = \varepsilon_B - E$

N-N self-interaction = $\varepsilon_N - E(k_x, k_y) = \varepsilon_N - E$

And B-N hopping integral= t

In matrix form the diagonal elements become: $\begin{bmatrix} \varepsilon_B - E & t \\ t & \varepsilon_N - E \end{bmatrix}$

Similarly, the interactions $(m-n1),(m-n2)$ form upper diagonal matrix $\begin{bmatrix} 0 & 0 \\ t & 0 \end{bmatrix}$and $(m-n3),(m-n4)$ form lower diagonal matrix $\begin{bmatrix} 0 & t \\ 0 & 0 \end{bmatrix}$. Therefore taking $\hat{a}_1$ and $\hat{a}_2$ into account the relation is given by:

$$E(\vec{K}) = \begin{bmatrix} 0 & t \\ 0 & 0 \end{bmatrix} e^{-ik\hat{a}_1} + \begin{bmatrix} 0 & t \\ 0 & 0 \end{bmatrix} e^{-ik\hat{a}_2} + \begin{bmatrix} \varepsilon_B - E & t \\ t & \varepsilon_N - E \end{bmatrix} + \begin{bmatrix} 0 & 0 \\ t & 0 \end{bmatrix} e^{ik\hat{a}_1} + \begin{bmatrix} 0 & 0 \\ t & 0 \end{bmatrix} e^{ik\hat{a}_2}$$

$$\begin{bmatrix} \varepsilon_B - E & t + te^{-ik\hat{a}_1} + te^{-ik\hat{a}_2} \\ t + te^{ik\hat{a}_1} + te^{ik\hat{a}_2} & \varepsilon_N - E \end{bmatrix}$$

$|E(K)| = 0$ (determinant of $E(K)$ is zero) gives the equation the following form :

$$(\boldsymbol{\varepsilon_B - E}).(\boldsymbol{\varepsilon_N - E}) - \boldsymbol{t^2}\,(\mathbf{1} + \boldsymbol{e^{-ik\hat{a}_1}} + \boldsymbol{e^{-ik\hat{a}_2}})(\mathbf{1} + \boldsymbol{e^{ik\hat{a}_1}} + \boldsymbol{e^{ik\hat{a}_2}}) = \mathbf{0}$$

$$\boldsymbol{\varepsilon_B\varepsilon_N - E\varepsilon_B - E\varepsilon_N + E^2 - t^2}\big(\mathbf{1} + \boldsymbol{e^{-ik\hat{a}_1}} + \boldsymbol{e^{-ik\hat{a}_2}}\big)\big(\mathbf{1} + \boldsymbol{e^{ik\hat{a}_1}} + \boldsymbol{e^{ik\hat{a}_2}}\big) = \mathbf{0} \quad (1.1)$$

Considering the part of the equation (1.1):

$$\big(\mathbf{1} + \boldsymbol{e^{-ik\hat{a}_1}} + \boldsymbol{e^{-ik\hat{a}_2}}\big)\big(\mathbf{1} + \boldsymbol{e^{ik\hat{a}_1}} + \boldsymbol{e^{ik\hat{a}_2}}\big)$$

$$\mathbf{1} + \boldsymbol{e^{-ik\hat{a}_1}} + \boldsymbol{e^{-ik\hat{a}_2}} + \boldsymbol{e^{ik\hat{a}_1}} + \boldsymbol{e^{-ik\hat{a}_1}e^{ik\hat{a}_1}} + \boldsymbol{e^{-ika_2}e^{ik\hat{a}_1}} + \boldsymbol{e^{ik\hat{a}_2}} + \boldsymbol{e^{ik\hat{a}_2}e^{-ik\hat{a}_1}} + \boldsymbol{e^{ik\hat{a}_2}e^{-ik\hat{a}_2}}$$

$$\mathbf{1} + \big(\boldsymbol{e^{ik\hat{a}_1}} + \boldsymbol{e^{-ik\hat{a}_1}}\big) + (\boldsymbol{e^{ik\hat{a}_2}} + \boldsymbol{e^{-ik\hat{a}_2}}) + \mathbf{1} + \boldsymbol{e^{-ik\hat{a}_2}e^{ik\hat{a}_1}} + \boldsymbol{e^{ik\hat{a}_2}e^{-ik\hat{a}_1}} + \mathbf{1}$$

$$\mathbf{3} + \mathbf{2}\cos\boldsymbol{k}.\hat{\boldsymbol{a}}_1 + \mathbf{2}\cos\boldsymbol{k}.\hat{\boldsymbol{a}}_2 + (\boldsymbol{e^{ik(\hat{a}_1 - \hat{a}_2)}} + \boldsymbol{e^{-ik(\hat{a}_1 - \hat{a}_2)}})$$

$$\mathbf{3} + \mathbf{2}(\cos\boldsymbol{k}.\hat{\boldsymbol{a}}_1 + \cos\boldsymbol{k}.\hat{\boldsymbol{a}}_2) + \mathbf{2}\cos\boldsymbol{k}(\hat{\boldsymbol{a}}_1 - \hat{\boldsymbol{a}}_2)$$

$$\mathbf{3} + \mathbf{2}(\mathbf{2}\cos\boldsymbol{k}\frac{(\hat{\boldsymbol{a}}_1 + \hat{\boldsymbol{a}}_2)}{\mathbf{2}}\cos\mathbf{k}\frac{(\hat{\boldsymbol{a}}_1 - \hat{\boldsymbol{a}}_2)}{\mathbf{2}}) + \mathbf{2}\cos\boldsymbol{k}(\hat{\boldsymbol{a}}_1 - \hat{\boldsymbol{a}}_2)$$

Substituting the values of the primitive vectors, $\hat{\boldsymbol{a}}_1 + \hat{\boldsymbol{a}}_2 = \sqrt{\mathbf{3}}\,\hat{\boldsymbol{a}}_x$ $\boldsymbol{and}$ $\hat{\boldsymbol{a}}_1 - \hat{\boldsymbol{a}}_2 = \hat{\boldsymbol{a}}_y$ leads the equation to as follows:

$$\left(1+e^{-ik\hat{a}1}+e^{-ik\hat{a}2}\right)\left(1+e^{ik\hat{a}1}+e^{ik\hat{a}2}\right)=3+4\ \cos k\ \frac{\sqrt{3}}{2}\hat{a}_x \cos k\frac{1}{2}\hat{a}_y+2\ (\ 2\ \cos^2 k\ \frac{1}{2}\hat{a}_y\ -1)$$

$$1+4\ \cos k\ \frac{\sqrt{3}}{2}\hat{a}_x \cos k\frac{1}{2}\hat{a}_y+4\ \cos^2 k\frac{1}{2}\hat{a}_y$$

Therefore equation (1.1) becomes,

$$\varepsilon_B\varepsilon_N-E\varepsilon_B-E\varepsilon_N+E^2-t^2(1+4\ \cos k\ \frac{\sqrt{3}}{2}\hat{a}_x \cos k\frac{1}{2}\hat{a}_y+4\ \cos^2 k\frac{1}{2}\hat{a}_y)=0$$

$$E^2-(\varepsilon_B+\varepsilon_N)E+[\varepsilon_B\varepsilon_N-t^2(1+4\ \cos k\ \frac{\sqrt{3}}{2}\hat{a}_x \cos k\frac{1}{2}\hat{a}_y+4\ \cos^2 k\frac{1}{2}\hat{a}_y)]=0$$

$$E(k_x,k_y)=\frac{(\varepsilon_B+\varepsilon_N)\pm\sqrt{[-(\varepsilon_B+\varepsilon_N)\}^2-4[\varepsilon_B\varepsilon_N\ -\ t^2\left(1\ +\ 4\ cos k\ \frac{\sqrt{3}}{2}\hat{a}_x cos k\frac{1}{2}\hat{a}_y+4\ cos^2 k\frac{1}{2}\hat{a}_y\right)]}}{2}$$

$$\frac{(\varepsilon_B+\varepsilon_N)}{2}\pm\frac{1}{2}\sqrt{[-(\varepsilon_B+\varepsilon_N)\}^2-4[\varepsilon_B\varepsilon_N\ -\ 4t^2\left(\frac{1}{4}\ +\ cos k\ \frac{\sqrt{3}}{2}\hat{a}_x cos k\frac{1}{2}\hat{a}_y+\ cos^2 k\frac{1}{2}\hat{a}_y\right)]}$$

$$\frac{(\varepsilon_B+\varepsilon_N)}{2}\pm\frac{1}{2}\sqrt{\varepsilon_B^2+\ \varepsilon_N^2+2\varepsilon_B\varepsilon_N\ -4\varepsilon_B\varepsilon_N\ +\ 16t^2\left(\frac{1}{4}\ +\ cos k\ \frac{\sqrt{3}}{2}\hat{a}_x cos k\frac{1}{2}\hat{a}_y+\ cos^2 k\frac{1}{2}\hat{a}_y\right)}$$

$$\frac{(\varepsilon_B+\varepsilon_N)}{2}\pm\frac{1}{2}\sqrt{(\varepsilon_B-\varepsilon_N)^2+\ 16t^2\left(\frac{1}{4}\ +\ cos k\ \frac{\sqrt{3}}{2}\hat{a}_x cos k\frac{1}{2}\hat{a}_y+\ cos^2 k\frac{1}{2}\hat{a}_y\right)}$$

Thus,

$$\mathrm{E}(\mathrm{k_x},\mathrm{k_y})=\frac{(\varepsilon_B+\varepsilon_N)}{2}\pm\sqrt{\frac{(\varepsilon_B-\varepsilon_N)^2}{4}+\ 4t^2\left(\frac{1}{4}\ +\ cos k\ \frac{\sqrt{3}}{2}\hat{a}_x cos k\frac{1}{2}\hat{a}_y+\ cos^2 k\frac{1}{2}\hat{a}_y\right)} \qquad (2.6)$$

Using this equation hexagonal shaped Brillouin zone of BN can be obtained, where out of six corners two of them are equivalent (the others can be written as one of these two plus a reciprocal lattice vector). These two special points are denoted with $\boldsymbol{K_+}$ and $\boldsymbol{K_-}$. Another high symmetry point is the one labeled with $\boldsymbol{M}$ in Fig. 2 (a). The center is denoted as Gamma $(\boldsymbol{\Gamma})$ valley.

(a) (b)

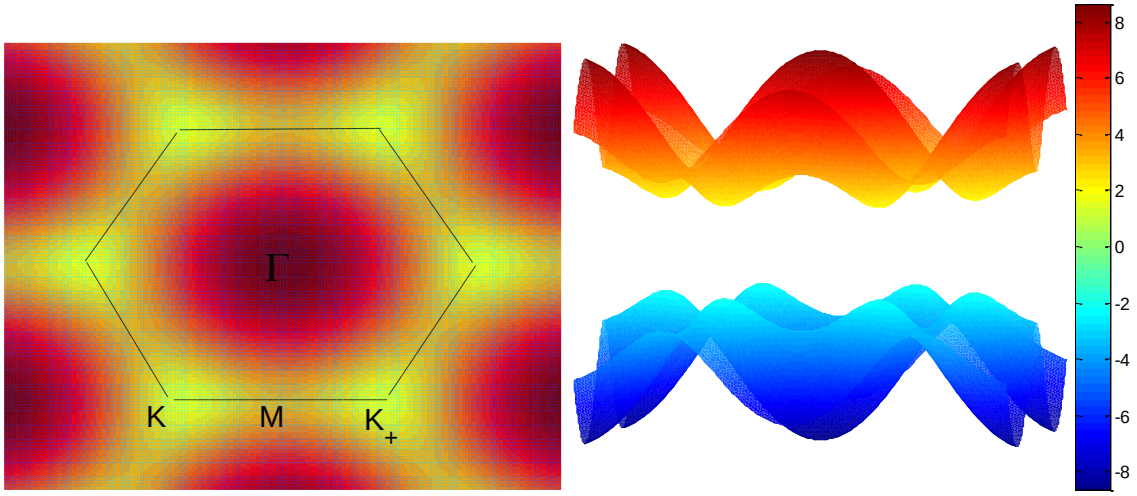

Fig. 2.3.4: (a) First Brillouin Zone(BZ) of H-BN. (b) Energy dispersion relation of H-BN.

2.4 Verification of Nearest TB model Calculated Band Structure with DFT:

In order to attain similar results from the nearest TB model as the first principles calculation, site energy and hopping integrals must be introduced in the TB model. In the absence of any of these two parameters edge effects cannot be obtained. From first principles calculation it has been observed that changes on the on-site energies and hopping integrals of the edge atoms due to edge charge distribution, are responsible for the distinct electronic structures and bandgap evolutions. Therefore, an edge-modified nearest TB approximation model has been developed which is not only capable of studying more intricate low dimensional Nano structures but also is cost-effective.[3-10]

2.4.1 Verifying Nearest TB model Calculated Band Structure of Graphene with DFT:

For Graphene only hopping integral needs to be taken into account as on-site energy is $\boldsymbol{\varepsilon = 0eV}$. In this case, the Highest Occupied Molecular Orbital (HOMO) and the Lowest Unoccupied Molecular Orbital (LUMO) touch at a certain point. But in the absence of the hopping integral the three family hierarchy becomes $E_g^{3p+2} > E_g^{3p+1} > E_g^{3p}$ ($\boldsymbol{p}$ is any integer), which contrasts with the resultant of first principles calculation which is $E_g^{3p} > E_g^{3p+1} > E_g^{3p+2}$. Since this property is valid when Nano Ribbon is taken into account, it is elaborately discussed in chapter 3 of this paper. However, in order to resolve the discrepancy between the DFT calculated HOMO and LUMO with that of the nearest TB model the value of hopping integral $\boldsymbol{t_{c-c}}$ must be increased to $\boldsymbol{t = -(1 + \Delta)}$, [where,$\boldsymbol{\Delta = 1.23}$].[3]

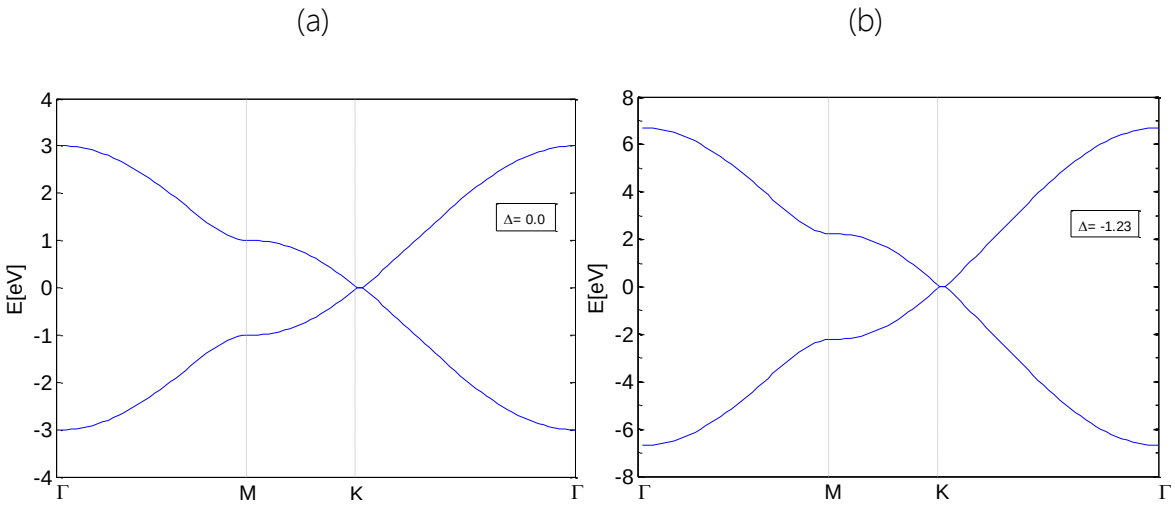

Fig. 2.4.1: Bandgap of AGNR (a) without edge modification. (b) with only modified hopping integral.

Therefore adjusted parameters and resultant bandgap are as follows:

On-site energy of C, $\boldsymbol{\varepsilon = 0eV}$

Hopping integral,$t_{C-C} = -2.23$ eV.

Lattice parameter, $a_{C-C} = 1.41\text{Å}$

Fermi energy level, $E_f = 0$ eV.

Energy gap, $E_g = 0$ eV.

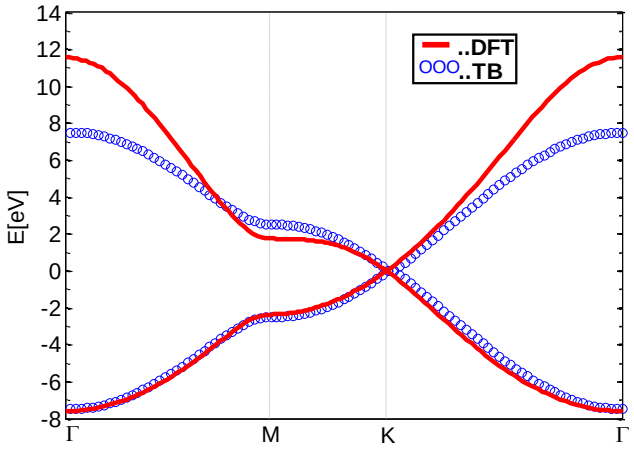

Fig 2.4.2: Comparison between HOMO and LUMO attained from DTF and stimulation.

2.4.2 Verifying Nearest TB model Calculated Band Structure of BN with DFT:

When the on-site energies and hopping integrals are not taken into account, $(\boldsymbol{\varepsilon_B = \varepsilon_N = 0 \,\&\, t = -1})$, the HOMO and LUMO touch at a certain point (Fig.2.4.3a). Moreover at these conditions there is discrepancy in the three family hierarchy. This discrepancy is best understood when Nano Ribbons are taken into account. However in order to adjust the HOMO and LUMO value of hopping integral must be altered to be, $\boldsymbol{t = -(1 + \Delta), [here\ \Delta = 1.3]}$.However only altering the hopping integral does not modify the band structure as the HOMO and LUMO still meet at a point (Fig. 2.4.3b).

From DFT calculation it has been observed that due to edge charge distribution of the edge atoms on-site energies change significantly. These on-site energies are mostly responsible for bandgap opening. As a result when on-site energies are applied to the nearest TB model (Fig. 2.4.3c) HOMO and LUMO do not touch, hence there exists a bandgap. These on-site energies can be obtained using the following equations:

$$\boldsymbol{\varepsilon_B = E_F + \sqrt{E_g^2/4}}$$

$$\boldsymbol{\varepsilon_N = E_F - \sqrt{E_g^2/4}}$$

Where $\boldsymbol{E_F}$ and $\boldsymbol{E_g}$ are obtained from DFT calculation. When only on-site energies $(\varepsilon_B = (0 + \delta\varepsilon_B) = 0.8614\ and\ \varepsilon_N = (0 + \delta\varepsilon_N) = -3.7712)$ are applied, the discrepancy of hierarchy reoccurs. In order to attain a bandgap with unchanged hierarchy, both the edge effects are employed together as shown in Fig. 2.4.3.(d). Therefore, using the edge-modified nearest TB approximation equivalent bandgap that equals DFT calculation is obtained. [3-8]

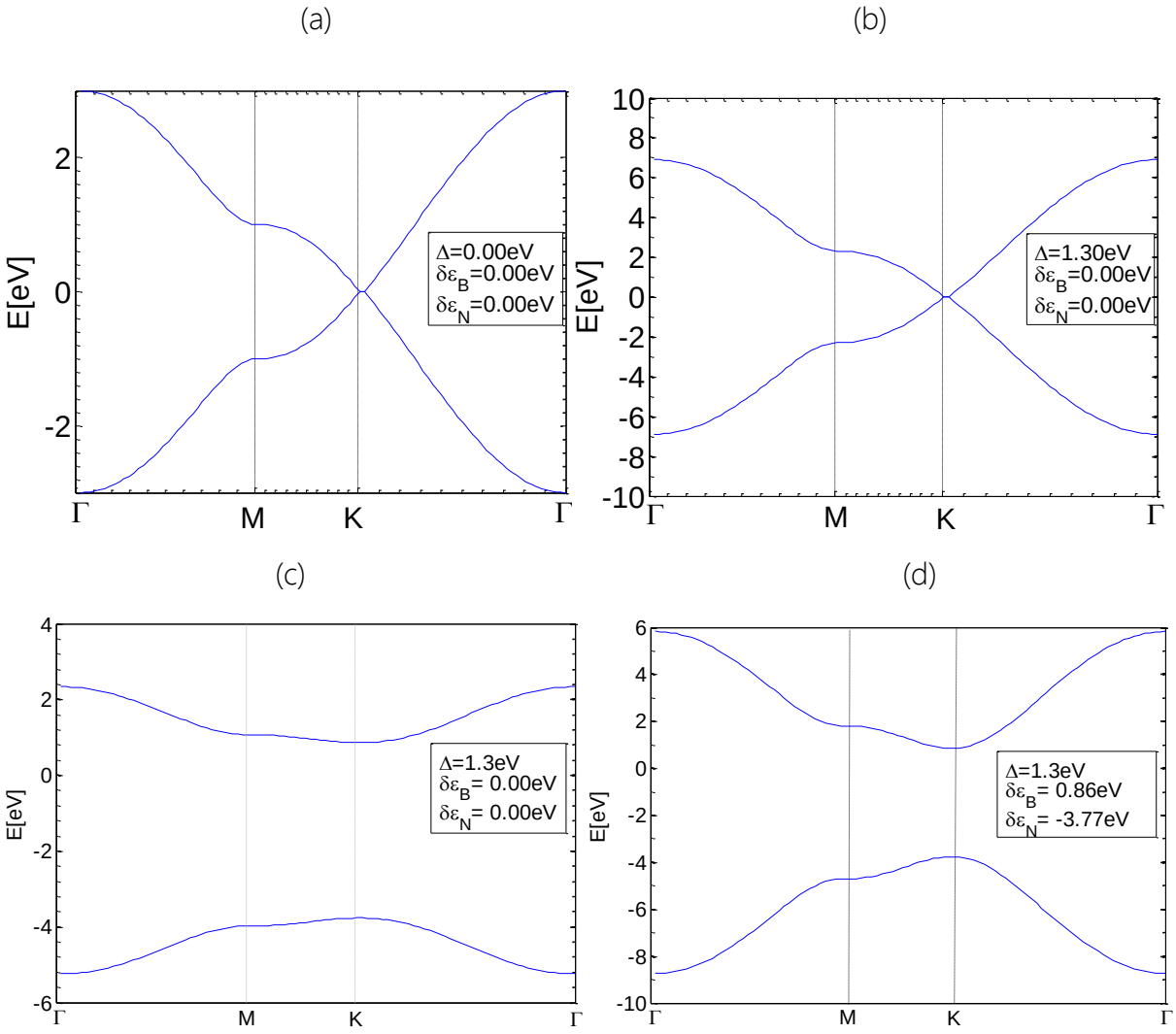

Fig. 2.4.3: Bandgap of ABNNR (a) without edge modification (b) with only modified hopping integral (c) with only modified on-site energies (d) with the modification of both hopping integrals and on-site energies.

The significance of on-site energies and hopping integrals can be further justified by adjusting the HOMO and the LUMO of TB Hamiltonian with the HOMO and LUMO of DFT calculation. The adjusted parameters and resultant bandgap are as follows:

On-site energy of B, $\varepsilon_B = 0.8614\text{eV}.$

On-site energy of N,$\varepsilon_N = -3.7712\ \text{eV}.$

Hopping integral,$t_{B-N} = -2.3\ \text{eV}.$

Lattice parameter, $a_{B-N} = 2.512\text{Å}$

Fermi energy level, $E_F = -1.4549\ \text{eV}.$

Energy gap, $E_g = 4.6326\ \text{eV}.$

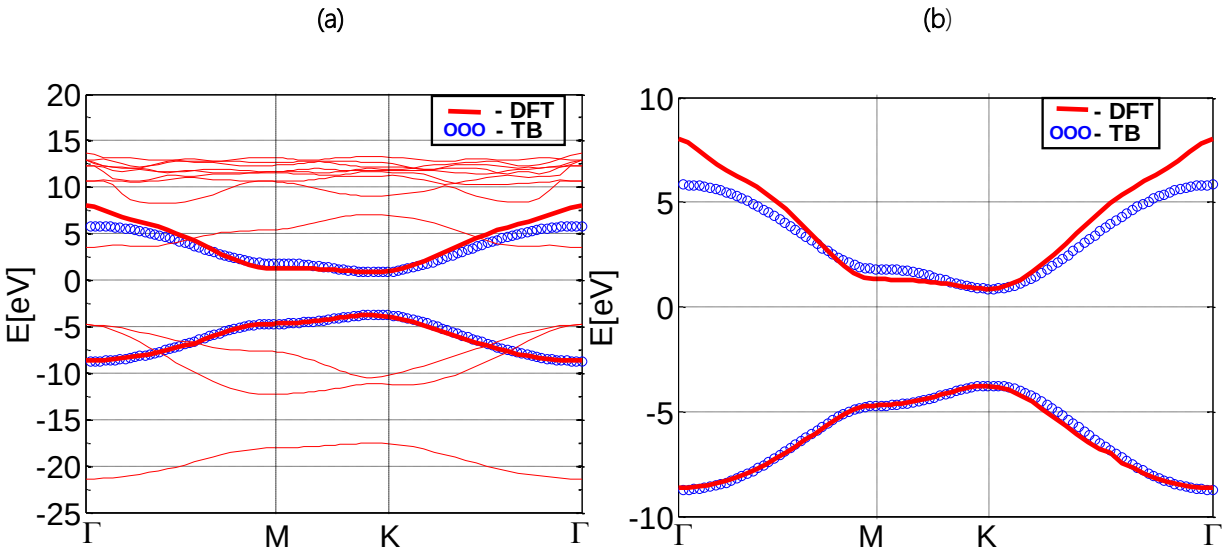

Fig. 2.4.5:(a) Comparison between HUMO and LUMO (b) Precise view of the comparison between attained from DFT and tight binding. HUMO and LUMO attained from DFT and tight binding.

Density of states (DOS), Local Electron Density and Electrostatic Potential Distribution of Graphene and Boron Nitride Unit Cell:

The density of states (DOS) of a particular system describes the number of energy states per unit energy per unit volume are available to be occupied. Density distributions are typically quasi-continuous. A high DOS at a particular energy means that there are many states available for occupation. If the DOS at a particular energy is zero then it means that no states can be occupied at that energy. Local variations, also known as Local Density of States (LDOS), are most often caused by local potential distribution (Electrostatic Difference

Potential) of the original system. If the DOS of an undisturbed system is zero then the LDOS can locally be non-zero due to the presence of a local potential.[21]

LDOS of a system can be obtained using the following equation:

$$G^R(E) = [(E + i\eta)I - H]^{-1}$$

Where,

I= is an identity matrix

$\eta = 1 \times 10^{-6}$, a very small value to make the overall matrix hermitian

H= Hamiltonian matrix of the system

Integrating LDOS over the spatial region we can get DOS of the system. We can calculate electron density from DOS figure as only the states below the Fermi level are occupied. An unit cell, Density of states, Local electron density and Electrostatic potential distribution are shown below for both Graphene and Boron Nitride.

(a)

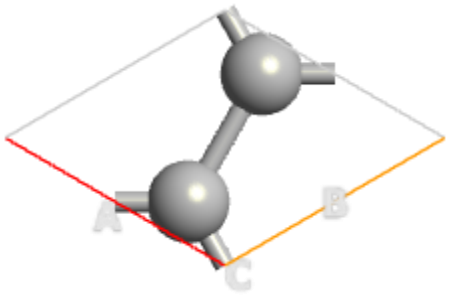
A
B
C

(b)

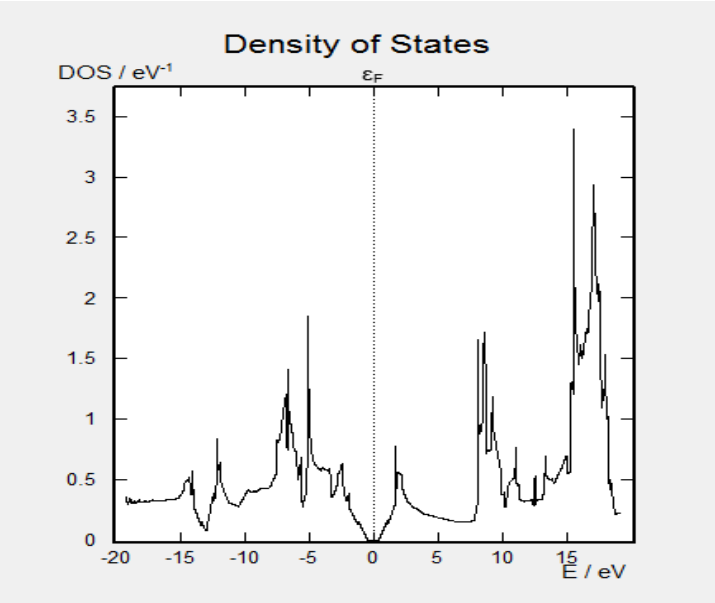
Density of States
DOS / eV-1
εF
3.5
3
2.5
2
1.5
1
0.5
0
-20
-15
-10
-5
0
5
10
15
E / eV

(c)

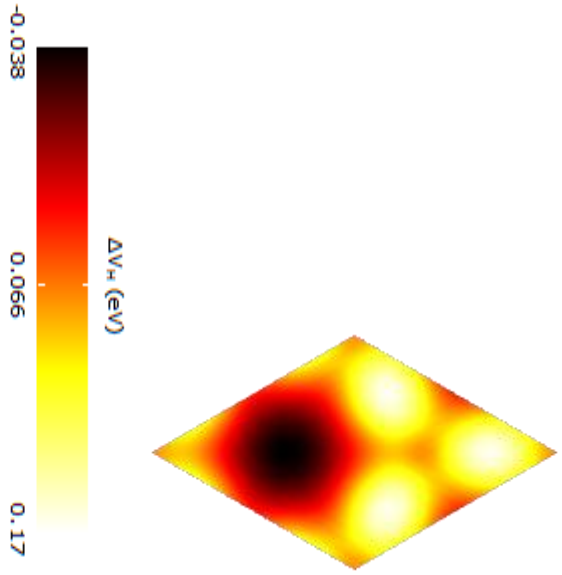
-0.038
0.066
0.17
ΔVH (eV)

(d)

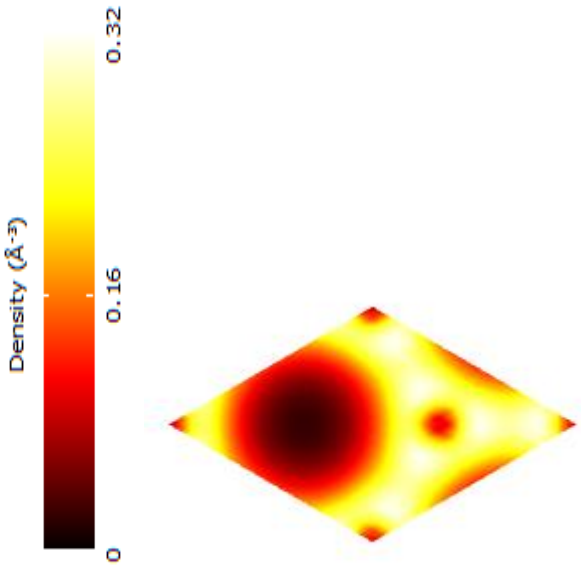

Fig.2.4.6:(a)unit cell of (b) density of states (c) electrostatic difference potential (d) electron density for Graphene.

(a) (b)

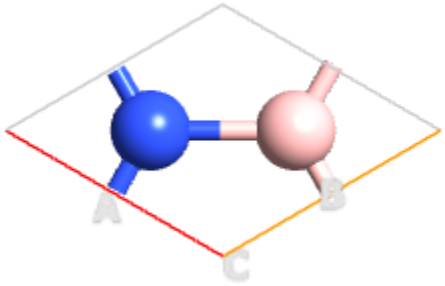

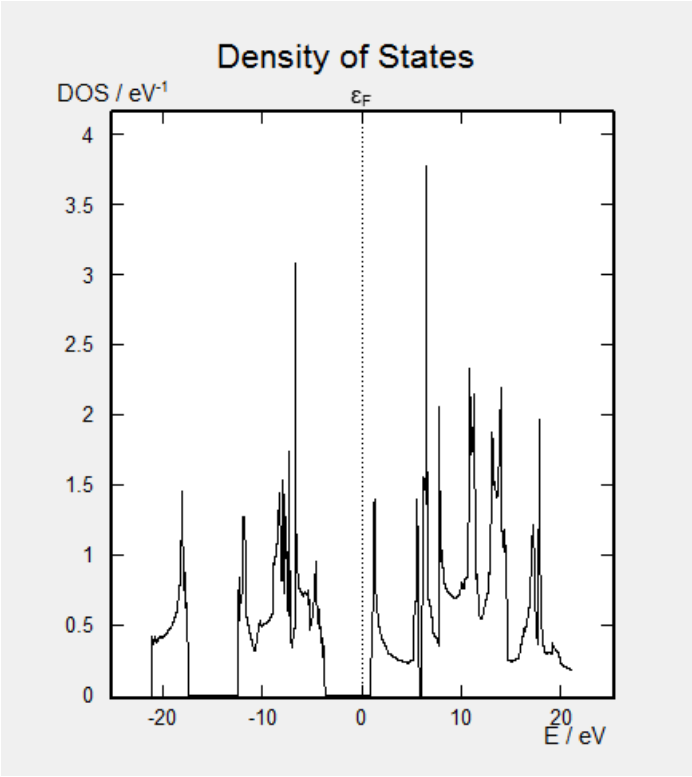

(c)

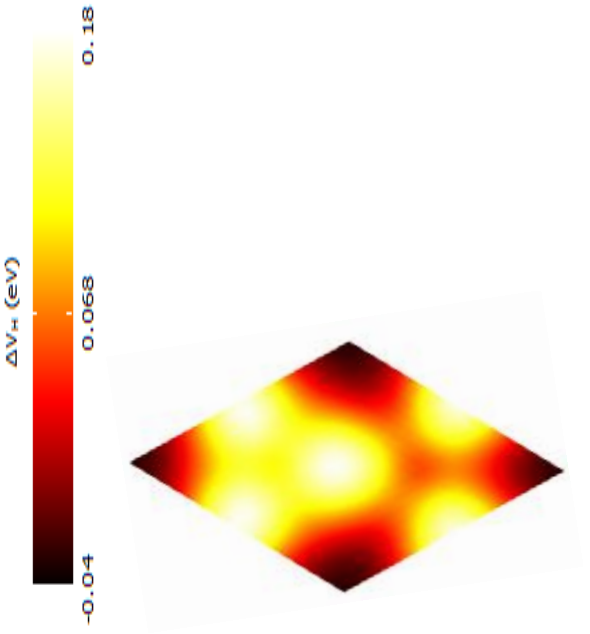

(d)

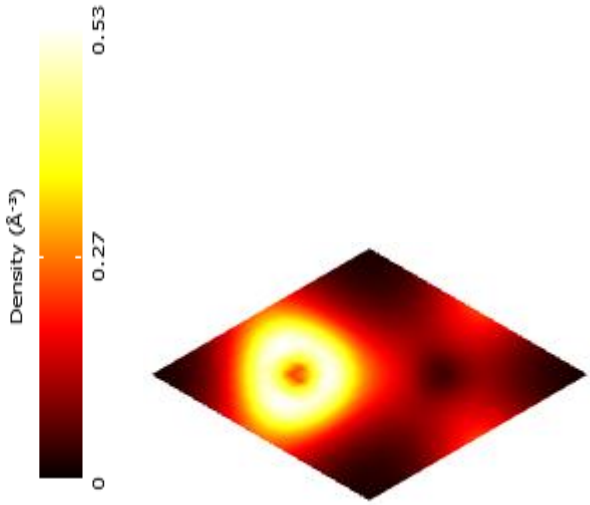

Fig.2.4.7:(a)unit cell of (b) density of states (c) electrostatic difference potential (d) electron density for BN.

2.5 Summary of the following Chapter:

In this chapter the bandgap of Graphene and BN have been examined in order to evaluate the metallic behavior of Graphene atoms and semiconductor-like behavior of BN atoms. Their Bravais lattice, E_K dispersion relation as well as Brillouin zone have been evaluated. Moreover, the effect of the on-site energies has been discussed elaborately. In addition the DOS representation has been incorporated to understand the electrostatic difference potential as well as electron density.

Though on-site energies can be evaluated using a single unit cell, such derivation falls to successfully evaluate the three family hierarchy of any Nano Ribbon. Thus the effects of fabricating these Nano scale materials into ribbons and the impact of hierarchy have been discussed in the next chapter.

Chapter 3: Graphene Nano Ribbons (GNR) and Boron Nitride Nano Ribbons (BNNR)

Nano Ribbon refers to a Nano structure in the form of a ribbon. Materials, when striped into a few nanometers width form Nano Ribbons exhibiting novel electronic properties. The electronic states of such Ribbons are largely a subject to the edge structures. Depending on these edge structures, Nano Ribbons are either Armchair or Zigzag. Suitable nano-structures for making a ribbon with different narrow widths can be made experimentally either by micromechanical cleavage (cutting mechanically exfoliated Graphene or BN) or by patterning epitaxial grown Nano structures. Previously only Graphene was used to fabricate such ribbons. Since BN features analogous structure as graphene it has triggered new scientific investigation. Among the immense applications of BNNR and GNR, the possibility of opening a tunable bandgap when GNR is embedded in BNNR, is the focus of this paper. [5]

3.1 Graphene Nano Ribbons (GNR):

Graphene Nano Ribbons (GNRs), also known as Nano Graphene Ribbons or Nano Graphite Ribbons, are defined as strips of Graphene with ultra-thin width (less than 50 nm). When a Graphene sheet is cut in such a manner that it forms a narrow strip, then the resulting structure is called GNR.

Such ribbons are formed by periodic repetition of Graphene junctions and have honeycomb arrangements, which lead to edge functionalization and more importantly bandgap opening. Depending on the cutting direction, these Graphene junctions or GNRs

are either Armchair-shaped or spin-polarized Zigzag-shaped. Fig. 3.1(a) and Fig. 3.1 (b) show the two types of nanoribbons and also define the unit cells of Armchair and Zigzag Graphene nanoribbons respectively. In investigations using the nearest TB model it is usually assumed that the dangling bonds are passivated by hydrogen atoms and do not contribute to the electronic structure near the Fermi level. Moreover, it has been observed that carbon-carbon distance has a crucial effect on the π -orbit coupling.

Armchair Graphene Nano Ribbons (AGNR):

Armchair Graphene Nano Ribbons (AGNR) do not have localized edge states, but their band gap is a function of the width. Therefore, with varying width AGNR is likely to encounter bandgap opening. Another reason for the opening of a band gap is edge distortion resulting from relaxation. The changes in position due to relaxation are again very small. The two edge atoms are shifted towards the nanoribbon and each other by almost 10^{-2} Å. The effect on the inner atoms is almost 10^{-3} Å or less. However, width has most impact on the three family hierarchy of band gap and can be categorized as follows $E_g^{3p} > E_g^{3p+1} > E_g^{3p+2}$ (where, p is any integer). $N = 3p, 3p+1 \; and \; 3p+2$ equal the number of dimer lines and characterize the width of the nanoribbon.[5-9]

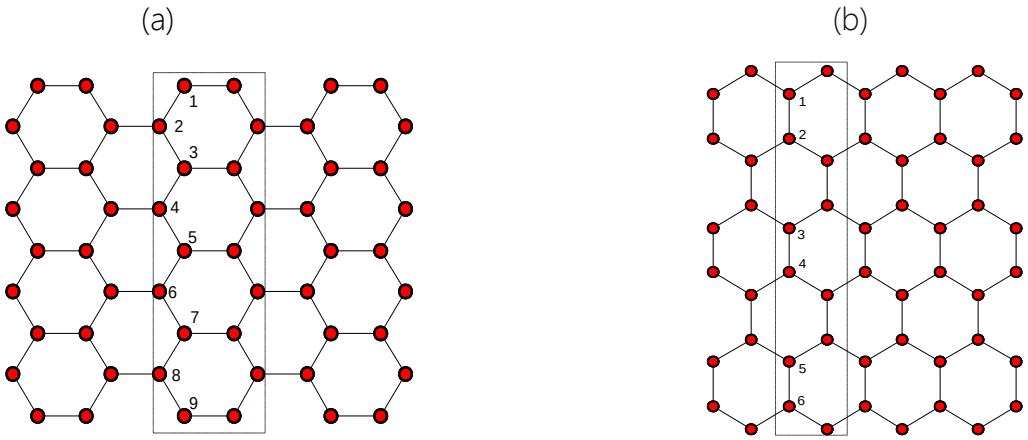

Fig. 3.1: Graphene Nano Ribbons (a) Armchair GNR (AGNR). (b) Zigzag GNR (ZGNR).

Zigzag Graphene Nano Ribbons (ZGNR):

It is well known from theoretical as well as experimental studies that Zigzag terminated Graphene Nano Ribbons feature localized edge states. These states decay exponentially into the bulk with the penetration length being a function of the *k* vector along the edge. Fig. 3.1(b) shows the unit cell of a ZGNR. Zigzag nanoribbon have two zero energy bands. The corresponding states are localized on each edge and only live on the sub-lattice which belongs to the outermost atom. [6-7]

3.2 Boron Nitride Nano Ribbons (BNNR):

Hexagonal BN (h-BN), also known as "white graphite" due to its similar structure and properties as graphite, was discovered in the same century as Graphene. But with credit to its lower cost and abundance in nature Graphene grabbed more attention than BN. However, BN has superior mechanical and thermal conducting properties. In contrast to zero bandgap

of Graphene, BNNRs exhibit wide bandgap suitable for semiconductors, optoelectronics and also dielectric substrate for high-performance graphene electronics. Thus, Graphene sandwiched by monolayer BN is predicted to have a tunable bandgap without sacrificing its mobility.

When a BN sheet is cut in such a manner that it forms a narrow strip with width less than 50nm, then the resulting structure is called BNNR. Such ribbons are formed by periodic repetition of BN junctions and also exhibit honeycomb arrangements as Graphene. These ribbons lead to edge functionalization and bandgap opening. Like Graphene Armchair-shaped or spin-polarized Zigzag-shaped BNNR are defined depending on the cutting direction. Fig. 3.2(a) and Fig. 3.2 (b) show the two types of nanoribbons and also define the unit cells of Armchair and Zigzag BNNR respectively. The bandgap opening in BNNR with respect to width increase has been calculated using the nearest TB model and evaluated using the DFT calculation based on first principles calculation. [1-2, 9-14]

Armchair BN Nano Ribbons (ABNNR):

BNNRs with armchair shaped edges on both sides are classified by the number of BN dimer lines across the ribbon width. The atoms at the two edges are saturated by H atoms. In analogy to AGNR, ABNNR encounters bandgap opening with varying width. Taking on-site energies and hopping integrals into account, successful fabrication of ABNNR also leads to a three family hierarchy of band gap: $E_g^{3p+1} > E_g^{3p} > E_g^{3p+2}$ (where, p is any integer). Thus for both AGNR and ABNN, bandgap increases for the width index of $N_{B=}N_{N=}3p$ and 3p+1 and decreases for the width index $N_B = N_N = 3p + 2$. Where, $N_B = N_N = 3p, 3p + 1$ and $3p + 2$ equals the number of dimer lines and characterize the width of the nanoribbon. [3-7]

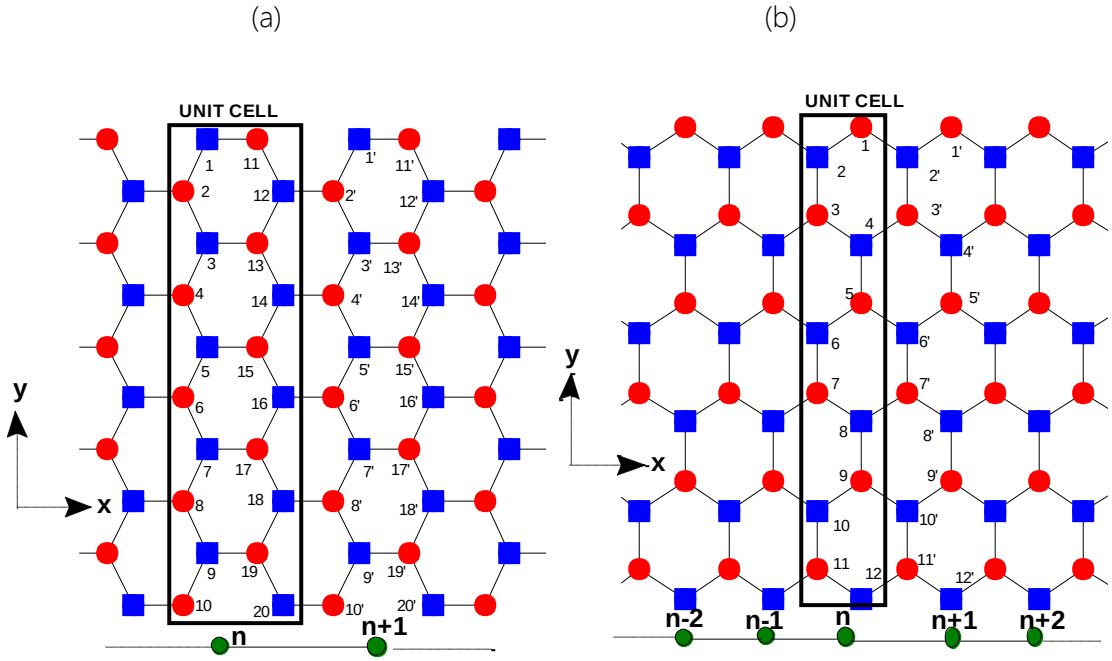

Fig.3.2:Boron Nitride Nanoribbon (a) Armchair BNNR structure (ABNNR). (b) Zigzag BNNR structure (ZBNNR).

Zigzag BN Nano Ribbons (ZBNNR):

Fig. 3.2(b) shows the unit cell of a ZBNNR. BNNRs with zigzag shaped edges on both sides are classified by the number of BN zigzag chains across the ribbon width. Like ABNNR, for ZBNNR the atoms at the two edges are also saturated by H atoms. Similar to the cases of ABNNRs, the on-site energies of edge atoms and the hopping integrals between the atoms near the edges play significant role in determining the band gap of ZBNNRs. Depending on the on-site energies ZBNNR are likely to encounter quantitatively larger band gap. [4-5]

3.3 Band structure observation of AGNR and ABNNR:

Using the DFT evaluated parameters in the nearest TB model the band structure and bandgap variation trends of both ABNNR and AGNR have been inspected. Since fabrication of Nano Ribbon is said to open a bandgap with changing width index, AGNR encounters bandgap opening for certain widths. In three family behavior, bandgap decreases with increasing width. However both DFT and nearest TB model calculation of the width index $3p+2$ (p is any integer) have zero bandgap (Fig. 3.3 a(iii)).Therefore, it leads to the proclaimed hierarchy of $E_g^{3p} > E_g^{3p+1} > E_g^{3p+2}$, which is in harmony with the first principles calculation. The cogency of the statement is further illustrated by the following figures Fig. 3.3 where width index is p (in this case the value of p is considered to be 2). Thus when $N = 3p = 6$ obtained bandgap is $1.33eV$ (Fig.3.3 a(i)), for $N = 3p+1 = 7$ obtained bandgap is $1.267eV$ (Fig. 3.3a(ii)) and for $N = 3p+2 = 8$ bandgap obtained is $0eV$ (Fig. 3.3 a(iii)). Therefore when number of carbon atom is 6 the attained bandgap is highest among the three families. Bandgap decreased by $0.067eV$ as number of carbons in the ribbon was increased and finally became zero for the index $3p+2$. The found parameters and bandgap can be summarized in the following table:

Table .I
TB parameters and bandgap comparison of AGNR

TB parameters (eV)

ε	t_{NC}
0	2.2

AGNR bandgap (eV)

$N=6$	$N=7$	$N=8$
1.33	1.267	0

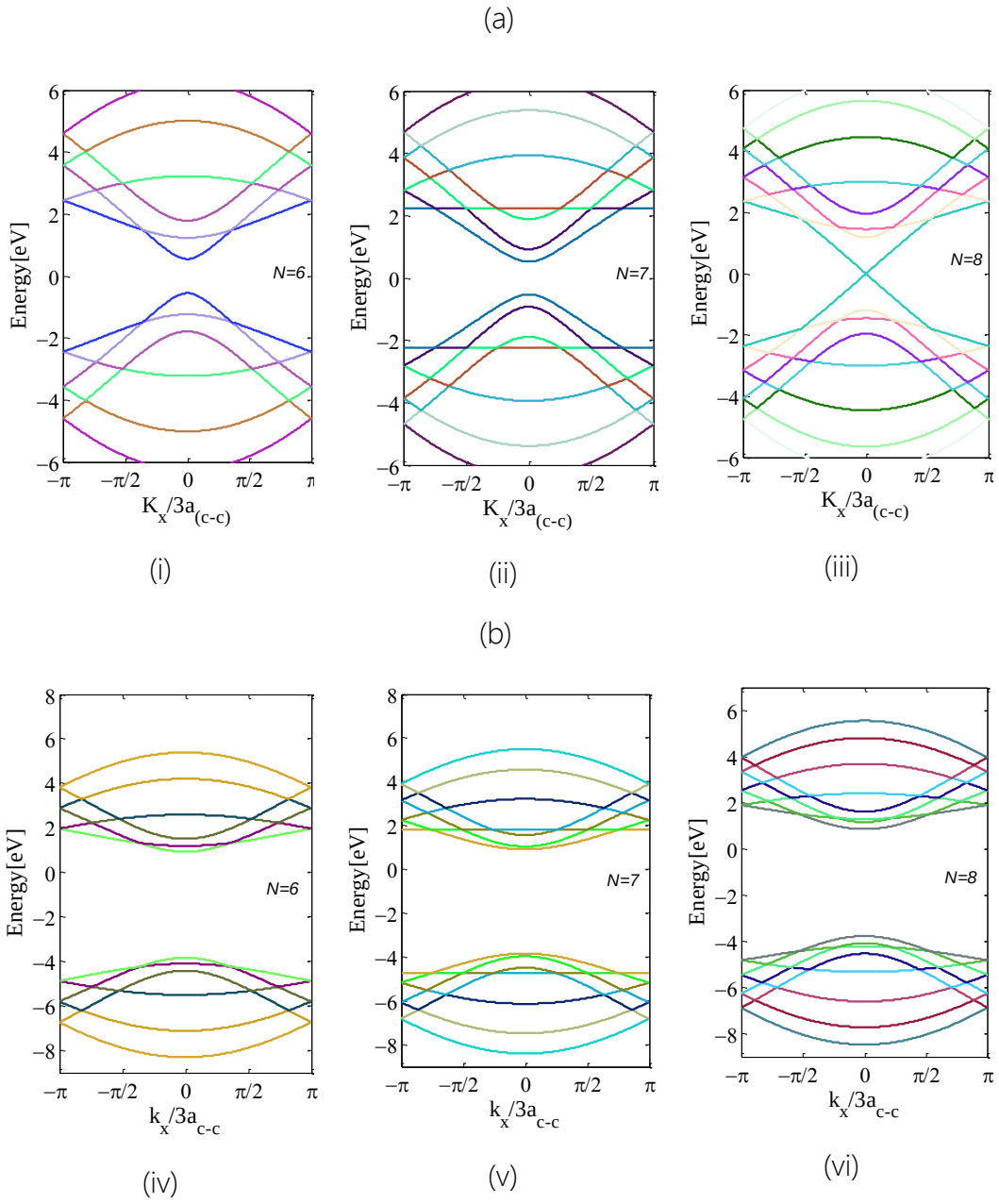

Fig. 3.3: (a) Band-structure of AGNR for varying ribbon width index, N;(i), N=6, (ii) N=7and (iii) N= 8, (b) Band-structure of ABNNR for varying ribbon width index, $N_B=N_N$; (iv) $N_B=N_N=6$, (v) $N_B=N_N=7$ and (vi) $N_B=N_N=8$.

In analogy with AGNR, ABNNR also encounters bandgap opening for certain widths. In ABNNR's three family behavior, bandgap increases with increase in width. The bandgap evolution of ABNNR has also been verified using both DFT and nearest TB model calculation. As claimed before ABNNR also exhibits a three family behavior but its three

family hierarchy is different from that of AGNR and it is as follows $E_g^{3p+1} > E_g^{3p} > E_g^{3p+2}$. Further illustration is provided in Fig. 3.3(b).Considering width index p to be $2, N_B = N_N = 3p = 6$ obtained bandgap is $4.7701eV$ (Fig. 3.3b(iv)), for $N_B = N_N = 3p + 1 = 7$ obtained bandgap is $4.88\ eV$ (Fig. 3.3 b(v)) and for $N_B = N_N = 3p + 2 = 7$ obtained bandgap is $4.63\ eV$ (Fig. 3.3 b(vi)). Therefore for ABNNR, the index $3p + 2$ exhibit lowest bandgap evolution.

Table II

TB Parameters and bandgap comparison of ABNNR

ABNNR Parameters (eV)		
ε_B	ε_N	t_{BN}
0.8614	−3.7712	2.3

ABNNR bandgap (eV)		
$N_B = N_N = 6$	$N_B = N_N = 7$	$N_B = N_N = 8$
4.7701	4.880	4.630

3.4 Band structure observation of ZGNR and ZBNNR:

Zigzag Nano Ribbons with controlled edge orientation can be fabricated by Scanning Tunneling Microscope (STM) lithography. Zigzag edges for GNR provide edge localized state with non-bonding molecular orbitals near the Fermi energy whereas in ZBNNRs π-electrons mainly accumulate on N atoms with high electronegativity. For both ZBNNR and ZGNR the band lines near the Fermi level are mainly dominated by the on-site energies. In these cases, the on-site Coulomb repulsion plays only a minor role in the electronic structures. Therefore,

ZGNR exhibits zero bandgap (Fig. 3.4(a)) as its on-site energy is zero and ZBNNR exhibits large bandgap, almost 4eV (Fig. 3.4(b)) due to its high on-site energies. Moreover, in contrast to ZGNR, the edge states of ZBNNRs are spin-unpolarized.

Table Ⅲ

TB parameters and bandgap of ZGNR and ZBNNR

ε_B (eV)	ε_N (eV)	ε (eV)	t_{BN} (eV)
0.8614	−3.7712	0	2.3

$ZGNR$ (eV)	$ZBNNR$ (eV)
0	~4.0

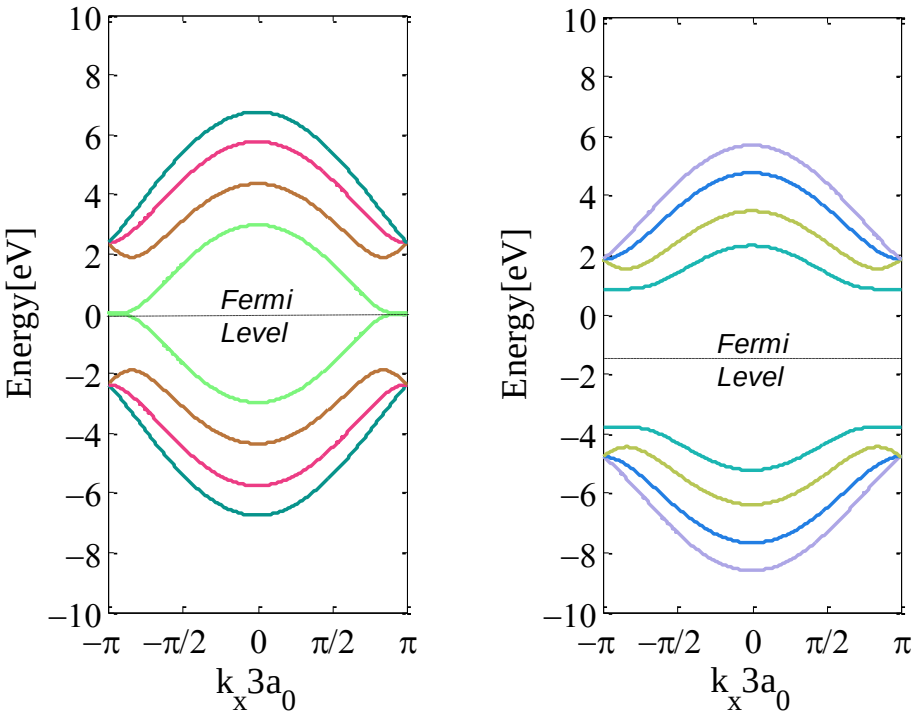

Fig. 3.4:(a) Fermi level and energy gap observation for ZGNR. (b) Fermi level and energy gap observation for ZBNNR.

3.5 Summary of the following Chapter:

Therefore, when stripped into a few nanometers width both AGNR and ABNNR exhibit semiconductor-like properties except for $3p + 2$ width index of AGNR. This leads to enormous possibilities of triggering new applications for ABNNR embedded AGNR. Further work of the paper is dedicated towards the investigation of the application of opening a tunable bandgap for any width index of both ABNNR and AGNR.

Chapter 4: Boron Nitride Nano Ribbons (BNNR) Embedded Graphene Nano Ribbons (GNR)

H-terminated GNRs require breaking of bonds whereas BNNRs exhibit quantitatively different properties due to large ionicities of B and N atoms. Thus BNNR confined GNRs form a continuous 2D atomistic layer that does not require any breaking of bonds and also provides a large enough current for transistor application. [17-22] Due to BNNR's large on-site energies, it contributes highly in causing charge redistribution at the edges of BNNR embedded GNR. The effect are most prominent for ABNNR embedded AGNR. Through this work we claim that AGNR encounters tunable bandgap when embedded in BNNR regardless of its ribbon width. [4]

4.1 Band Structure of ABNNR embedded AGNR:

The zero bandgap of GNR is used as contact in electronic devices but for transistor mechanism, semiconductor-like behavior is required. Nano scale semiconductor devices of GNRs represent a densely packed parallel array of semiconducting AGNRs. However this semiconducting behavior is limited to certain width indexes of the ribbon. But for BNNR, no such limitations are encountered due to the charge distribution of the edge atoms leading to large on-site energies of the matter. For AGNR there is no on-site energy (or almost close to zero on-site energy), as a result when fabricated in ribbons in fails to behave like semiconductor for the width index 3p+2 (p is any integer). This deficiency can be overcome when AGNR is embedded in ABNNR, as the effective charge distribution of BNNR edge atoms causes charge re-distribution in AGNR leading to tunable bandgaps for all width indexes.

Starting from the time independent Schrodinger's equation:

$$E(\vec{k})\psi(\vec{k},\vec{r}) = H_{op}\psi(\vec{k},\vec{r}) \qquad (4.1)$$

Where, H_{op} is the Hamiltonian operator, $E(\vec{k})$ and $\psi(\vec{k},\vec{r})$ are the eigen-energies and eigen-functions respectively in a ABNNR embedded AGNR and $\vec{k}$ and $\vec{r}$ represent the wavevector and position, respectively. The *j*-th eigen value $E_j(\vec{k})$ as a function of $\vec{k}$ is given by:

$$E_j(\vec{k}) = \frac{\langle\psi_j|H_{op}|\psi_j\rangle}{\langle\psi_j|\psi_j\rangle} = \frac{\int \psi_j{}^* H_{op}\psi_j d\boldsymbol{r}}{\int \psi_j{}^*\psi_j d\boldsymbol{r}} \qquad (4.2)$$

Because of the translational symmetry of the ABNNR embedded AGNR atoms in a ABNNR embedded AGNR lattice, the eigen-functions, $\psi_j(\vec{k},\vec{r})$ (j=1, 2, …, n), where *n* is the number of Bloch wave functions can be written as a linear combination of Bloch orbital basis functions $u_m(\vec{r})$

$$\psi_j(\vec{k},\vec{r}) = \sum_{j'=1}^{n} \phi_{jj'}(\vec{k})u_{j'}(\vec{k},\vec{r}) \qquad (4.3)$$

Where $\phi_{jj'}(\vec{k})$ gives the coefficients to be determined, and $u_{j'}(\vec{k},\vec{r})$ satisfies

$$u_{j'}(\vec{k},\vec{r}+\vec{a_i}) = u_{j'}(\vec{k},\vec{r}) \qquad (4.4)$$

Substituting (4.3) into (4.2) and changing subscripts we obtain

$$E_i(\vec{k}) = \frac{\sum_{j,j'}^{n} \phi_{ij}^*\phi_{ij}\langle u_j|H_{op}|u_{j'}\rangle}{\langle u_j|u_{j'}\rangle} = \frac{\sum_{j,j'}^{n} H_{jj'}(\vec{k})\phi_{ij}^*\phi_{ij'}}{\sum_{j,j'}^{n} S_{jj'}(\vec{k})\phi_{ij}^*\phi_{ij'}} \qquad (4.5)$$

Here the integrals are over the Bloch orbitals, and are called the transfer integral matrix and overlap integral matrix, respectively, which are defined as

$$H_{jj'}(\vec{k}) = \langle u_j|H_{op}|u_{j'}\rangle,\ S_{jj'}(\vec{k}) = \langle u_j|u_{j'}\rangle \qquad (4.6)$$

$H_{jj'}(\vec{k})$and $S_{jj'}(\vec{k})$ have fixed values, for a given value of $\vec{k}$, and the coefficient ϕ_{ij}^* is optimized so as to minimize $E_i(\vec{k})$. Taking a partial derivative with respect to ϕ_{ij}^* to obtain the local minimum condition gives,

$$\frac{\partial E_i(\vec{k})}{\partial \phi_{ij}^*} = \frac{\sum_{j'=1}^{n} H_{jj'}(\vec{k})\phi_{ij'}}{\sum_{j,j'=1}^{n} S_{jj'}(\vec{k})\phi_{ij}^*\phi_{ij'}} - \frac{\sum_{i,j'=1}^{n} H_{jj'}(\vec{k})\phi_{ij}^*\phi_{ij'}}{\left(\sum_{j,j'=1}^{n} S_{jj'}(\vec{k})\phi_{ij}^*\phi_{ij'}\right)^2}\sum_{j'=1}^{n} S_{jj'}(\vec{k})\phi_{ij'} = 0 \qquad (4.7)$$

Multiplying both sides of (3.7) by $\sum_{j,j'=1}^{n} S_{jj'}(\vec{k})\,\phi_{ij}^*\phi_{ij'}$ and substituting (3.5) into the second term

$$\sum_{j'=1}^{n} H_{jj'}(\vec{k})\phi_{ij'} = E_i(\vec{k})\sum_{j'=1}^{n} S_{jj'}(\vec{k})\phi_{ij'} \qquad (4.8)$$

Now,

$$H\phi_i = E_i(\vec{k})S\phi_i \qquad (4.9)$$

Where ϕ_i is a column vector defined by

$$\phi_i = [\phi_{i1}\phi_{i2} \ldots \phi_{in}]^T \qquad (4.10)$$

(4.9) only has a non-zero solution when

$$det[H - E_i(\vec{k})S] = 0 \qquad (4.11)$$

(4.11) is called the secular equation, whose solution gives all eigenvalues $E_i(\vec{k}), i = 1, 2, .. n$ of for agiven wave vector $\vec{k}$.

If ABNNR embedded AGNR channel comprises of $M + 1$ unit cells then both the Hamiltonian, H and overlap matrixes,S are $(M + 1) \times (M + 1)$ tridiagonal matrix, where each element of these matrixes is also $2N \times 2N$ constant matrix. For Hamiltonian matrix lower diagonal, diagonal and upper diagonal elements are H_b, H_a, H_c respectively. Similarly for

overlap matrix lower diagonal, diagonal and upper diagonal elements are S_b, S_a, S_c respectively.

$$E\begin{bmatrix} S_{0,0} & S_{0,1} & & & & & & \\ S_{1,0} & & & & & & & \\ & & S_{i-1,i} & & & & & \\ & S_{i,i-1} & S_{i,i} & S_{i,i+1} & & & & \\ & & S_{i+1,i} & & & & & \\ & & & & & & S_{M-1,M} & \\ & & & & & S_{M,M-1} & S_{M,M} & \end{bmatrix}\begin{Bmatrix} \varphi_0 \\ \vdots \\ \varphi_{i-1} \\ \varphi_i \\ \varphi_{i+1} \\ \vdots \\ \varphi_M \end{Bmatrix} =$$

$$\begin{bmatrix} H_{0,0} & H_{0,1} & & & & & & \\ H_{1,0} & & & & & & & \\ & & H_{i-1,i} & & & & & \\ & H_{i,i-1} & H_{i,i} & H_{i,i+1} & & & & \\ & & H_{i+1,i} & & & & & \\ & & & & & & H_{M-1,M} & \\ & & & & & H_{M,M-1} & H_{M,M} & \end{bmatrix}\begin{Bmatrix} \varphi_0 \\ \vdots \\ \varphi_{i-1} \\ \varphi_i \\ \varphi_{i+1} \\ \vdots \\ \varphi_M \end{Bmatrix} \qquad (4.12)$$

For *i*-th unit cell φ_i is the $2N$-dimensional vector representing the wave function at the*i*-thunit cell. The Hamiltonians, $H_{i,i-1}$, $H_{i,i}$, $H_{i,i+1}$ and overlap matrixes $S_{i,i-1}$, $S_{i,i}$, $S_{i,i+1}$ are all $2N \times 2N$ constant matrixes. Due to periodicity of the structure we can write: $H_{i,i} = H_a$, $H_{i,i-1} = H_b$, $H_{i,i+1} = H_c = H_b^*$ and $S_{i,i} = S_a$, $S_{i,i-1} = S_b$, $S_{i,i+1} = S_c = S_b^*$

Taking *i*-th row of (4.12) we have

$$H_{i,i-1}\varphi_{i-1} + H_{i,i}\varphi_i + H_{i,i+1}\varphi_{i+1} - E\left(S_{i,i-1}\varphi_{i-1} + S_{i,i}\varphi_i + S_{i,i+1}\varphi_{i+1}\right) = 0 \qquad (4.13)$$

Because of the property of Bloch function we have $\varphi_i = e^{ikn}(k = k_x/d)$ where d is the distance between two neighboring unit cells. For armchair ABNNR embedded A-GNRs, $d = 3a_{c-c}$ and in case of Z-GNRs, $d = \sqrt{3}a_{c-c}$. Substituting φ_i into (4.13) we have

$$\det\left[H_b e^{-ik} + H_a + H_c e^{ik} - E\left(S_b e^{-ik} + S_b + S_c e^{ik}\right)\right] = 0 \qquad (4.14)$$

Equation (4.14) gives $2N$ solutions for $E(k)$ corresponding to N sub-bands of the dispersion relation. In the case of first nearest approximation without orbital overlap, S_b, S_c are empty matrix and S_a becomes an identity matrix.

Using the following equation the H_A, H_B and H_C matrixes required for determining the bandgap of ABNNR embedded AGNR are formed. With proper on-site energy and hopping integrals of both the matters in contact the DFT obtained bandgap is reproduced in the approximated nearest TB model.

The H matrixes are as follows:

(a)

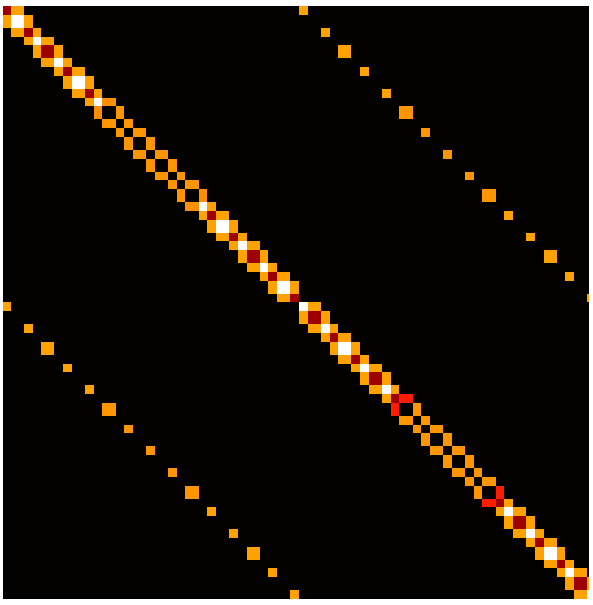

(b)

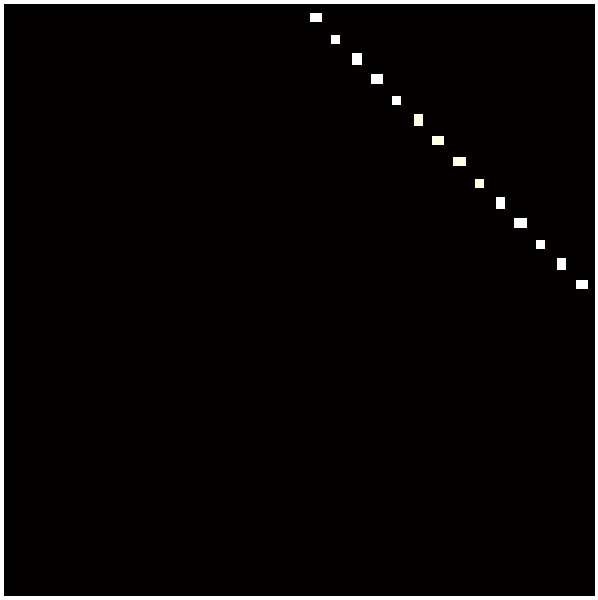

(c)

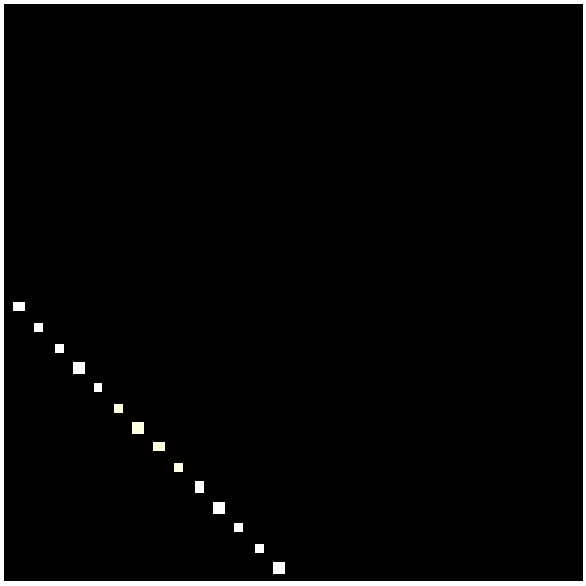

Fig. 4.1.1: (a) Ha matrix (b) Hb matrix (c) Hc matrix

Where, $-(t=-2.3)$, $-(\varepsilon=0.8614)$, $-(t=-1.57)$, $-(t=-2.23)$

4.1.1 Band Structure Comparison of AGNNR and ABNNR embedded AGNR for semiconducting width index

$3p$ and $3p+1$width indexes are known as semiconducting width index. For all AGNR with these width indexes, there is a bandgap opening. The bandgap attained for 3p is always greater than that of $3p+1$,. But for ABNNR with a hierarchy of $E_{3p+1}^{g} > E_{3p}^{g} > E_{3p+2}^{g}$the bandgap obtained from $3p+1$index is greater than that of 3p. When AGNR is confined by ABNNR it follows its own hierarchy of $E_{3p}^{g} > E_{3p+1}^{g} > E_{3p+2}^{g}$. From here on ,AGNR confined by ABNNR will be denoted by A-C_xBN_y; where x and y represent width of AGNR and ABNNR respectively.

Comparing AGNR and ABNNR embedded AGNR for the value of width index $p = 3$, the bandgap obtained for AGNNR is $0.7728eV$ and for A-C_9BN_{20} is $0.8882eV$. Therefore, there is a bandgap opening of $0.1152eV$. Again for $3p + 1$, the bandgap obtained for AGNNR is $0.7428\ eV$ and for A-$C_{10}BN_{20}$ is $0.7434\ eV$. Therefore, there is a bandgap opening of $0.0006eV$.

(a) (b)

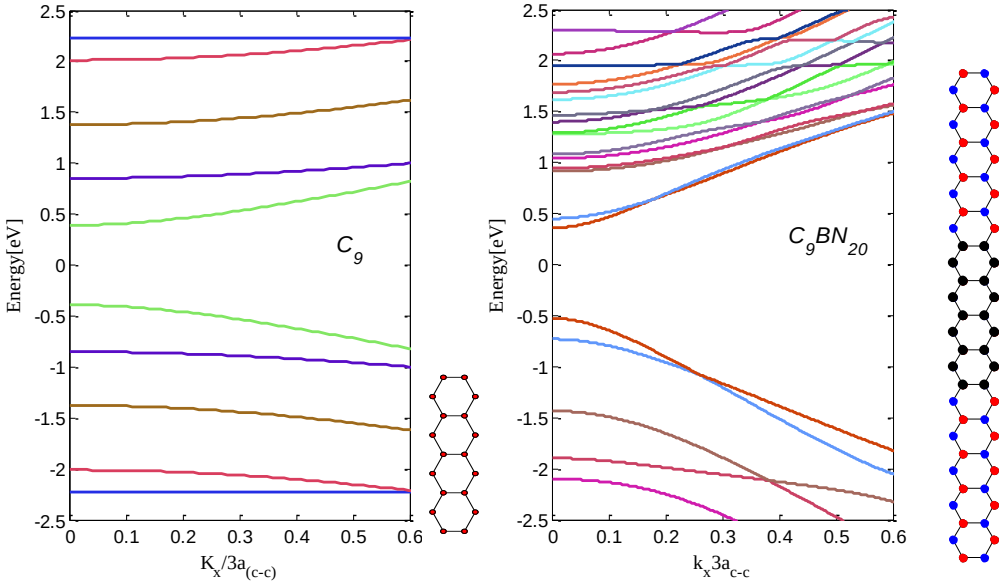

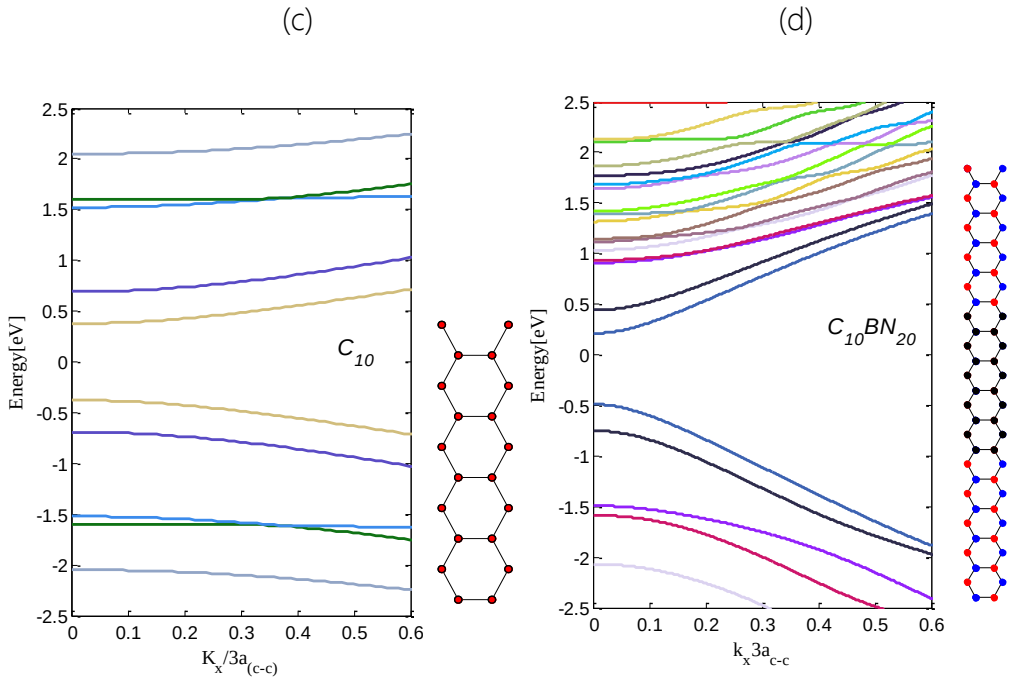

Fig. 4.1.2: Band Structure of (a) C_9, (b) A-C_9BN_{20}, (c) C_{10} and (d) A-$C_{10}BN_{20}$

4.1.2 Band Structure Comparison of AGNNR and ABNNR embedded AGNR for metallic width index:

3p+2 index in known as the metalic width index of AGNR as it results in zero bandgap like metals. For both AGNR and ABNNR embedded AGNR this index exhibits the lowest bandgap. For AGNR is has almost zero bandgap, but when embedded in ABNNR there is potential bandgap opening.

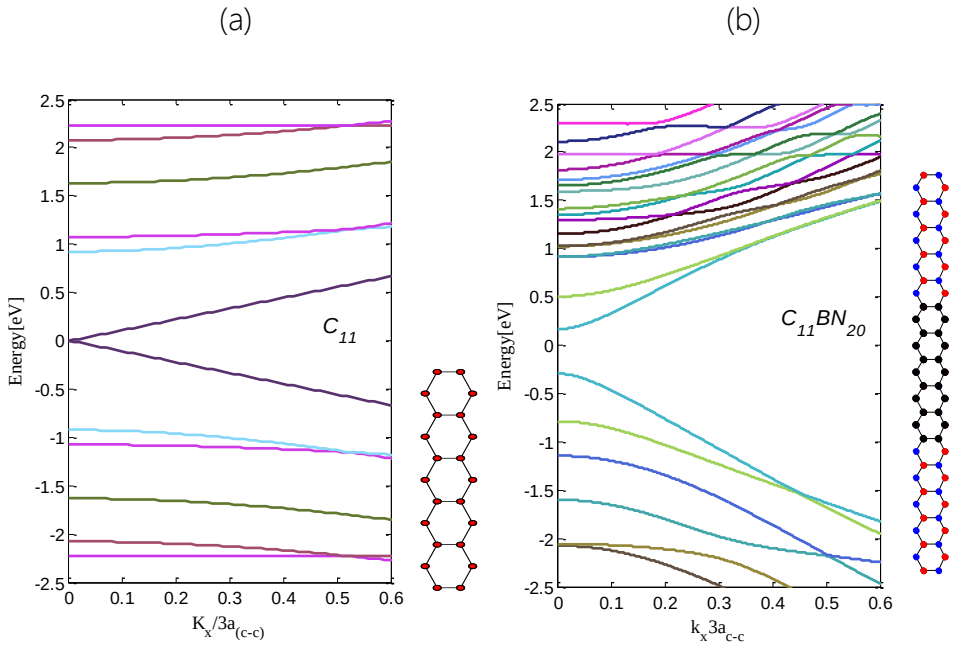

Fig. 4.1.3: Band Structure of (a) C_{11} and (b) A-$C_{11}BN_{20}$.

From the naerest TB model approximation it is evident that where C11 exhibits zero bandgap, A-$C_{11}BN_{20}$ exhibits a bandgap of $\mathbf{0.4577}eV$. Therefore leading to a potential bandgap opening of $\mathbf{0.4577}\ eV$.

4.2 Band Structure of ABNNR embedded AGNR using DFT:

In order to evaluate the bandgap obtained from the nearest TB approximation with that of the first principles calculation, an evaluation with respect to DFT is performed. Using this verification the parameters used in TB model are adjusted for most approximate results. The verification is performed for $3p\ and\ 3p+2$ width indexes. Parameters taken into account are ones that give most satisfying results for both the cases.

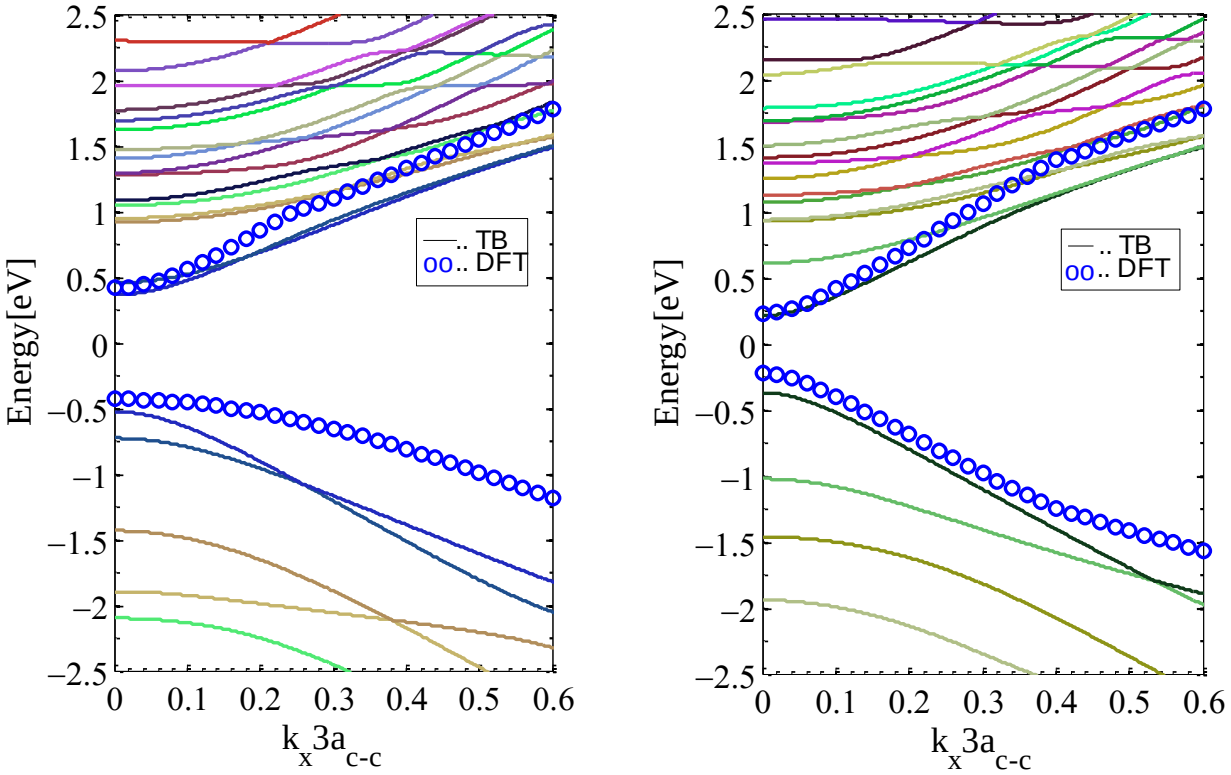

Fig. 4.2.1: Comparison between HOMO and LUMO attained from TB model and DFT calculation for (a) A-C_9BN_{20} and (b) A-$C_{11}BN_{20}$.

In research of the verification of semiconducting indexes, HOMO of both calculations matches more precisely than LUMO for the parameters stated in Table 4.1. However, these parameters were found best adjusted for HOMO and LUMO of both TB method and DFT of metallic ABBNR embedded AGNR.

Table: IV
BNNR confined GNR Parameters

$\varepsilon_B(eV)$	$\varepsilon_N(eV)$	$\varepsilon(eV)$	$t_{NC}(eV)$	$t_{BN}(eV)$	$t_{BC}(eV)$	$t_{CC}(eV)$
0.8614	−3.7712	0	2.2	2.3	1.57	2.23

For further justification of the following parameters the bandgaps obtained for both A-C_9BN_{20} and A-$C_{11}BN_{20}$ using DFT and the nearest TB model data comparison and graphical representation are taken into account.

Table V
Data Comparison of DFT vs TB Model for
A-C_9BN_{20} and A-$C_{11}BN_{20}$.

C_xBN_y	DFT simulated bandgap value (eV)	Bandgap obtained from Tight binding model (eV)
C_9BN_8	0.877399	0.9196
C_9BN_{12}	0.874632	0.8879
C_9BN_{16}	0.874474	0.8893
C_9BN_{20}	0.874124	0.8882
C_9BN_{24}	0.866751	0.7888
$C_{11}BN_8$	0.45699	0.4724
$C_{11}BN_{12}$	0.456267	0.4579
$C_{11}BN_{16}$	0.45624	0.4575
$C_{11}BN_{20}$	0.456241	0.4577
$C_{11}BN_{24}$	0.456261	0.4559

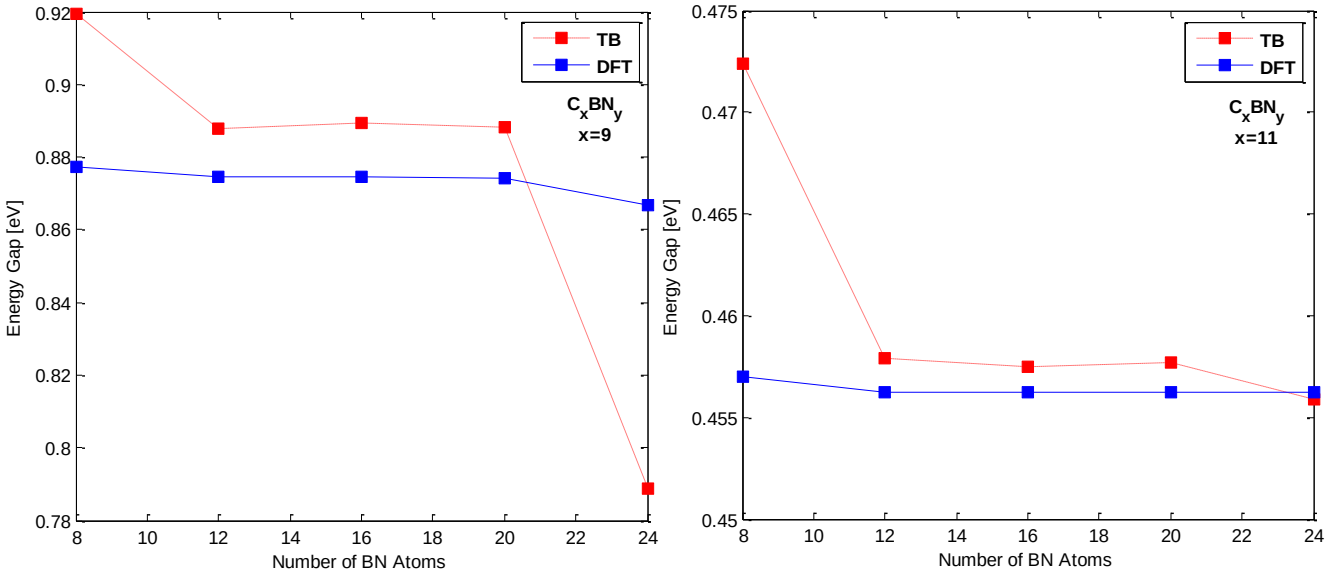

Fig. 4.2.2: Graphical Comparison between bandgaps obtained from TB model and DFT calculation for (a) A-C_9BN_{20} and (b) A-$C_{11}BN_{20}$.

After several alterations the parameters stated in Table.4.2.1 are attained. The resultant of the research indicates that bandgap obtained using the nearest TB model approximation has about $0.0003eV\ to\ 0.08\ eV$ difference from the DFT calculated bandgaps. Thus, these parameters have been used to investigate the bandgap for other width indexes of A-C_xBN_y and therefore a vast study has been conducted for the purpose.

4.3 An Extensive Analysis of the Band Structure of ABNNR embedded AGNR:

In order to understand the distinct variation trends of AGNR confined by ABNNR (A-C_xBN_y) a series of bandgap ranging from $x = 5\ to\ x = 20$ have been taken into account. For calculations simplicity the initial value of y is considered to be 8 and the value increases with an interval of 4 and continues up to 24. The value of y is taken up to the width of 24 as

A-C_xBN_y attains somewhat constant value of bandgap at that point. Afterwards bandgap remains unchanged regardless of the increase in y.

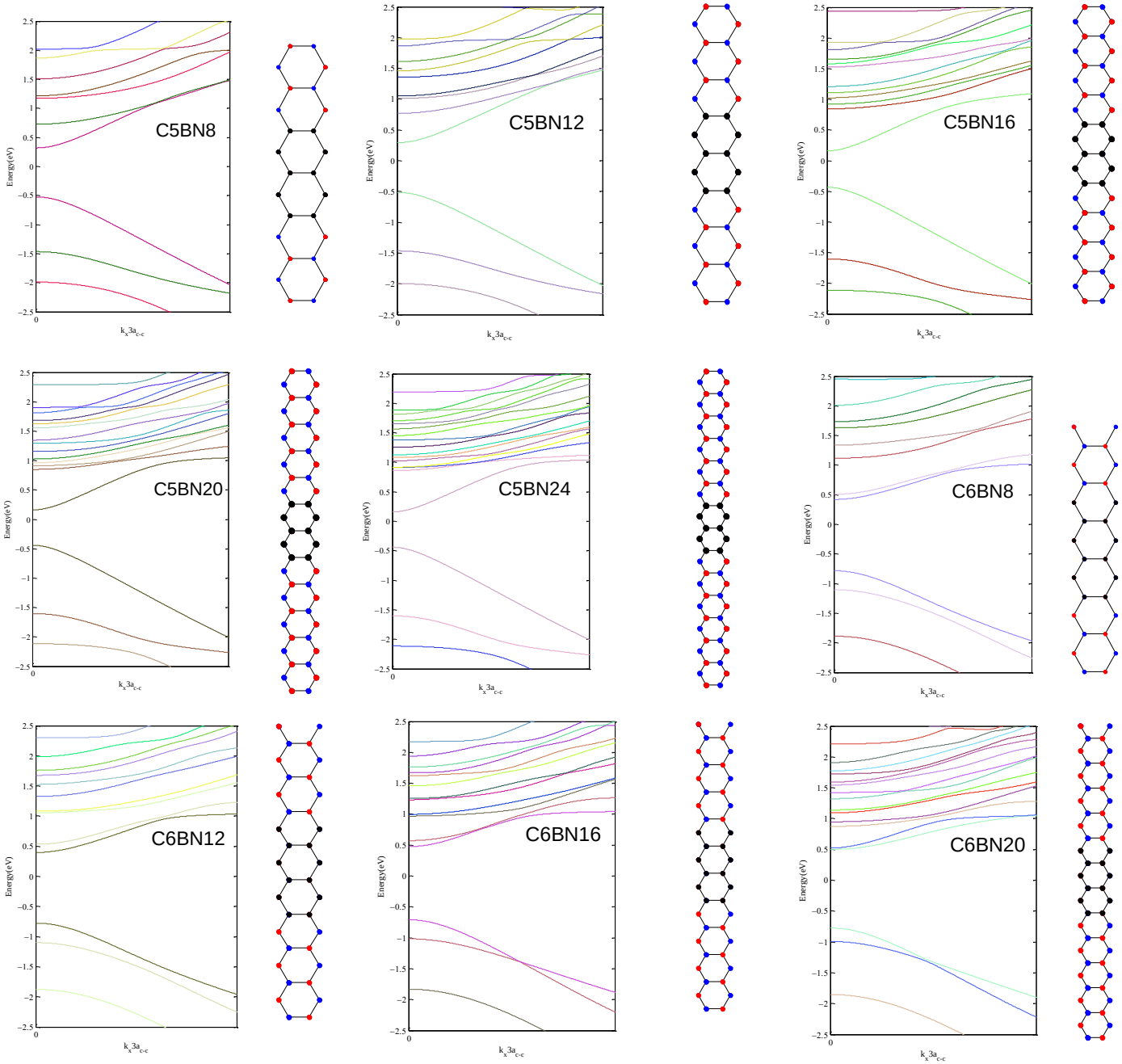

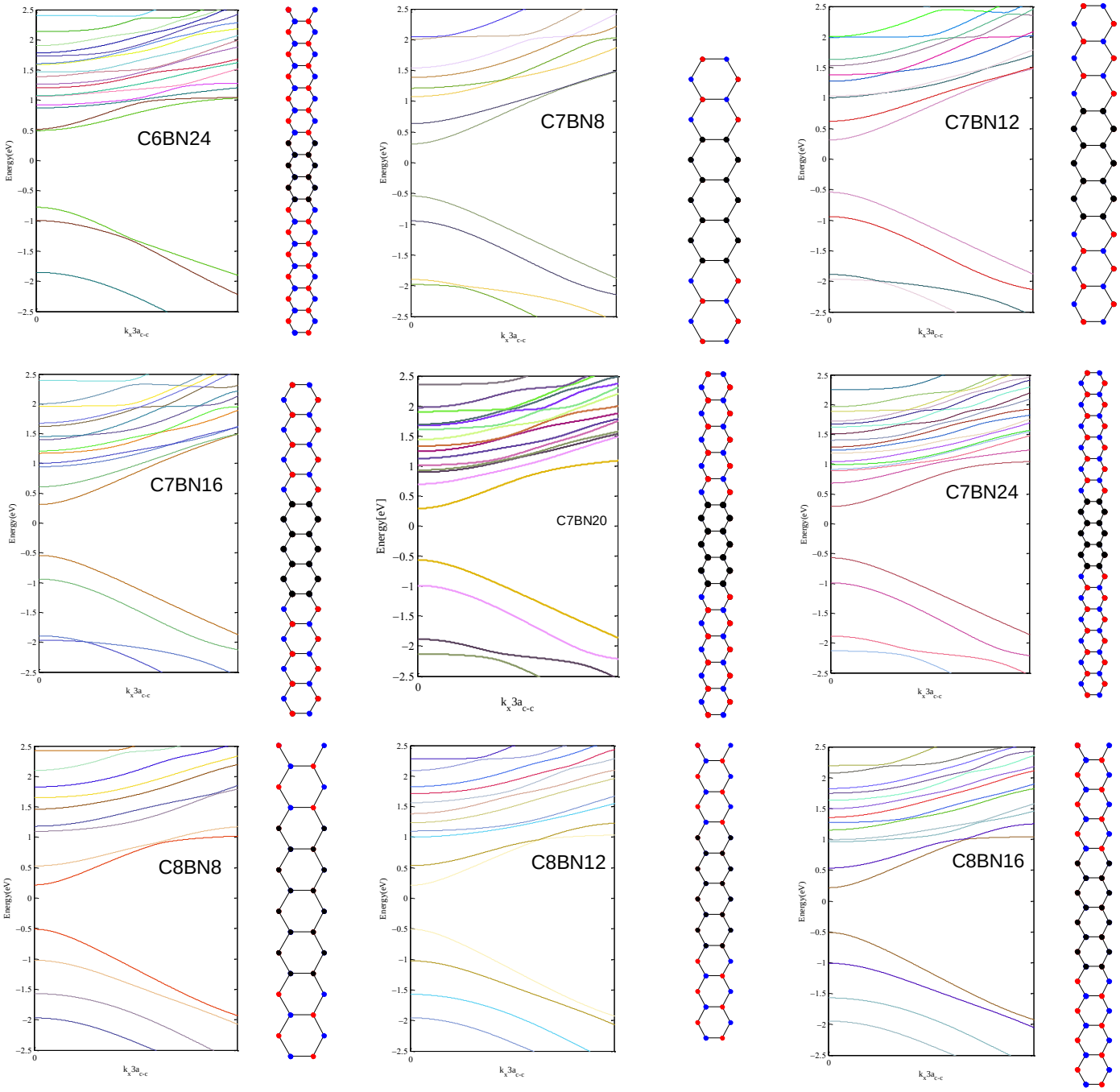
C6BN24
C7BN8
C7BN12
C7BN16
C7BN20
C7BN24
C8BN8
C8BN12
C8BN16
Energy(eV)
Energy[eV]
k_x 3a_c-c

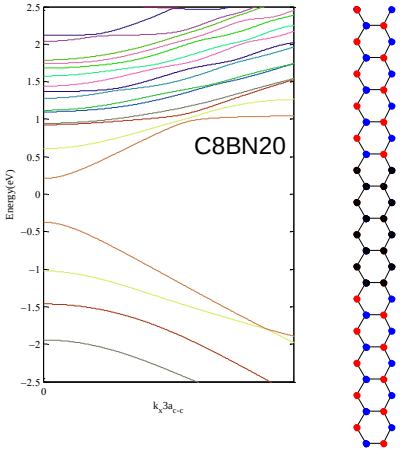
C8BN20
Energy(eV)
$k_x 3a_{c-c}$

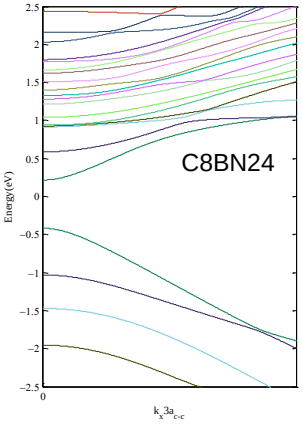
C8BN24
Energy(eV)
$k_x 3a_{c-c}$

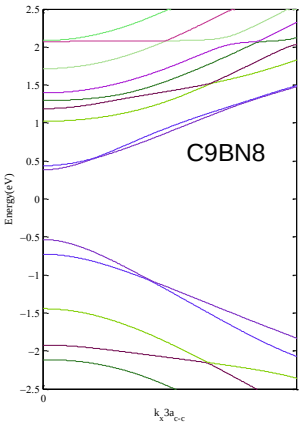
C9BN8
Energy(eV)
$k_x 3a_{c-c}$

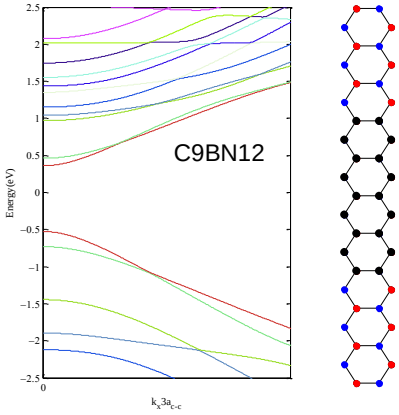
C9BN12
Energy(eV)
$k_x 3a_{c-c}$

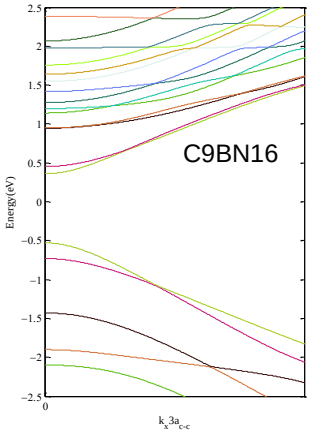
C9BN16
Energy(eV)
$k_x 3a_{c-c}$

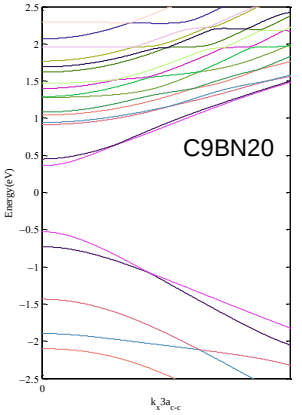
C9BN20
Energy(eV)
$k_x 3a_{c-c}$

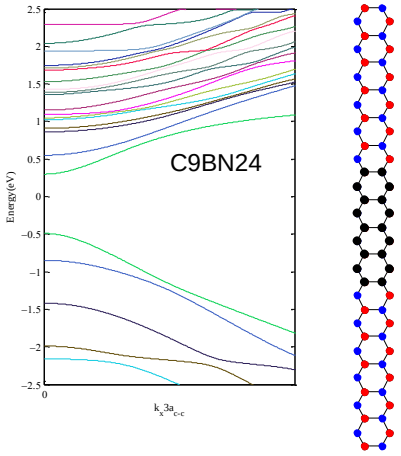
C9BN24
Energy(eV)
$k_x 3a_{c-c}$

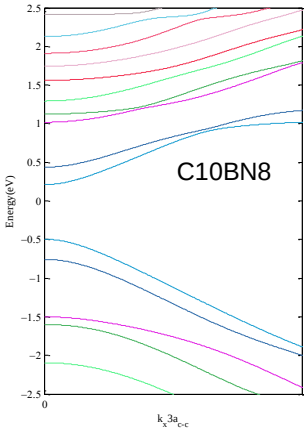
C10BN8
Energy(eV)
$k_x 3a_{c-c}$

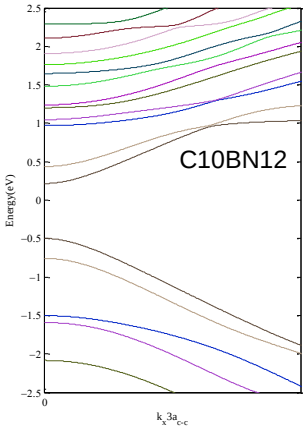
C10BN12
Energy(eV)
$k_x 3a_{c-c}$

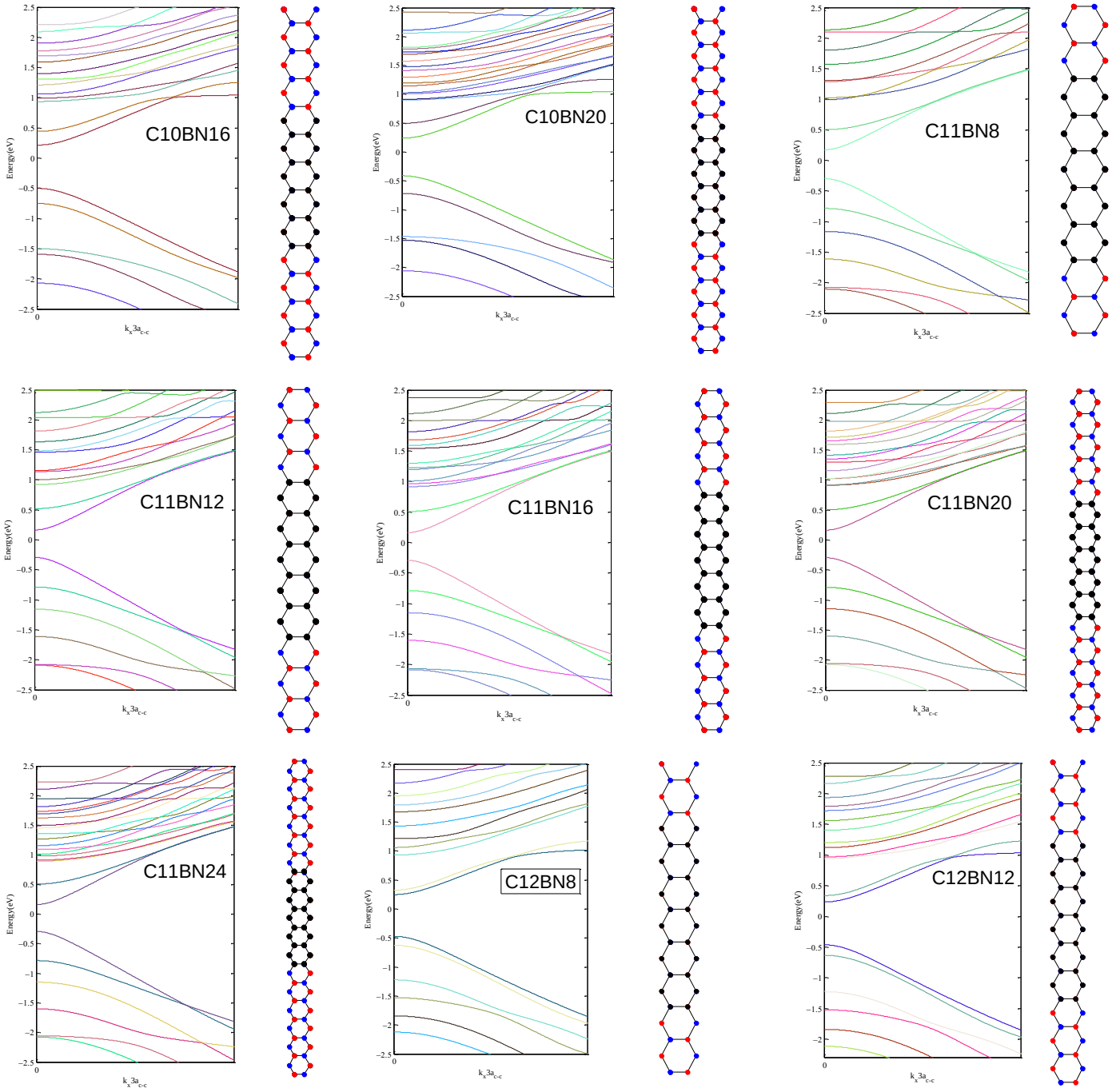
C10BN16
C10BN20
C11BN8
C11BN12
C11BN16
C11BN20
C11BN24
C12BN8
C12BN12
Energy(eV)
k_x3a_c-c

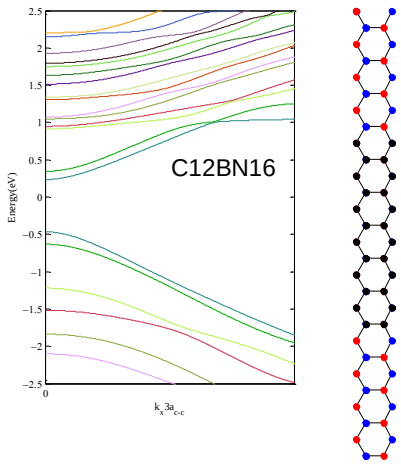
C12BN16
Energy(eV)
$k_x 3a_{c-c}$

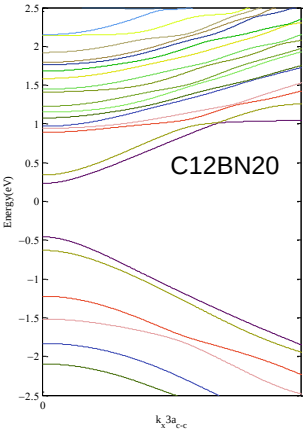
C12BN20
Energy(eV)
$k_x 3a_{c-c}$

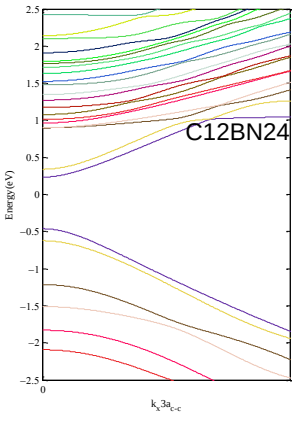
C12BN24
Energy(eV)
$k_x 3a_{c-c}$

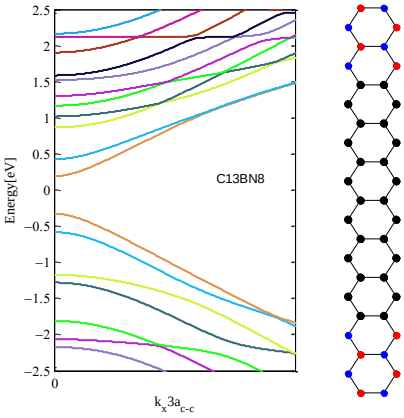
C13BN8
Energy[eV]
$k_x 3a_{c-c}$

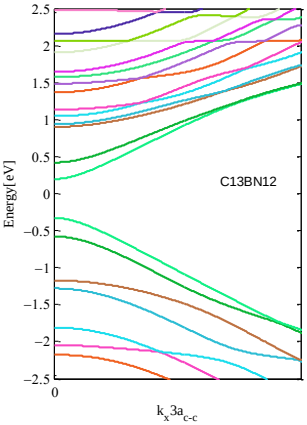
C13BN12
Energy[eV]
$k_x 3a_{c-c}$

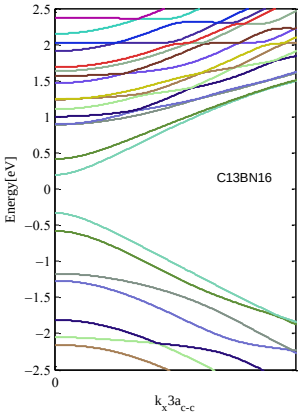
C13BN16
Energy[eV]
$k_x 3a_{c-c}$

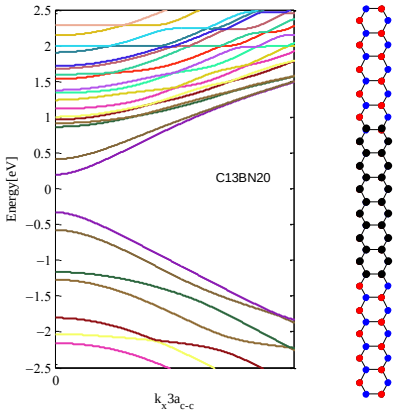
C13BN20
Energy[eV]
$k_x 3a_{c-c}$

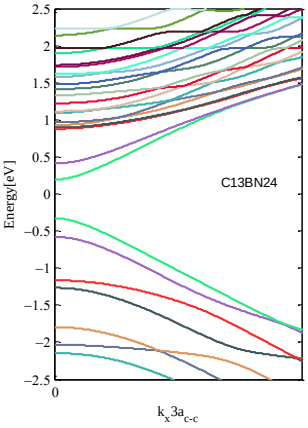
C13BN24
Energy[eV]
$k_x 3a_{c-c}$

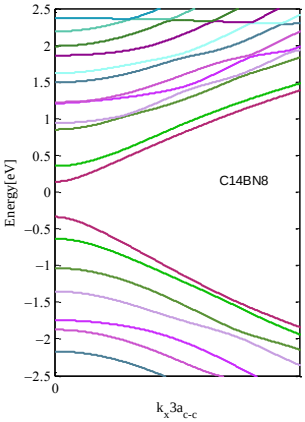
C14BN8
Energy[eV]
$k_x 3a_{c-c}$

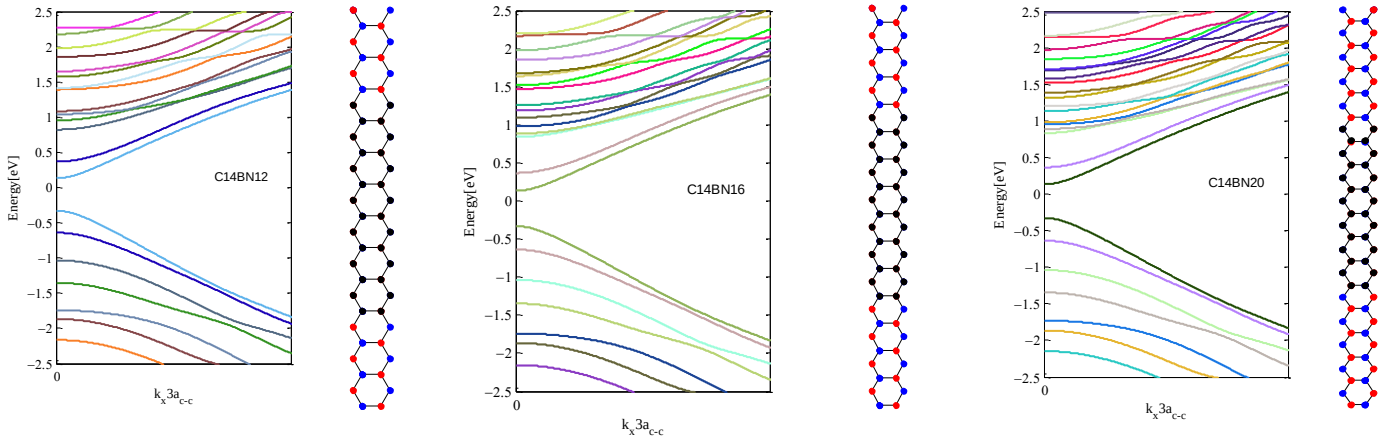
C14BN12
C14BN16
C14BN20
Energy[eV]
$k_x 3a_{c-c}$

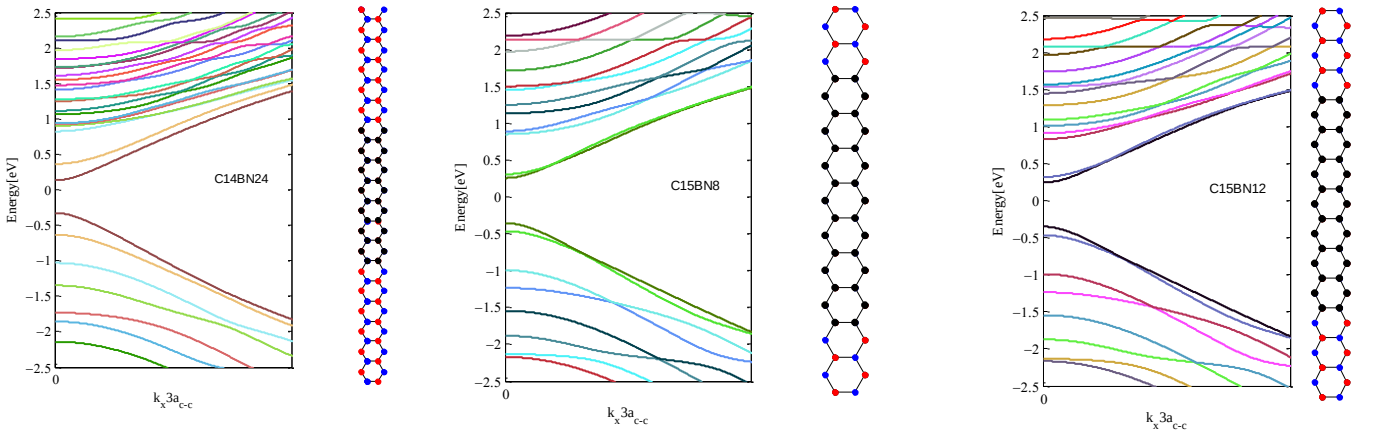
C14BN24
C15BN8
C15BN12
Energy[eV]
$k_x 3a_{c-c}$

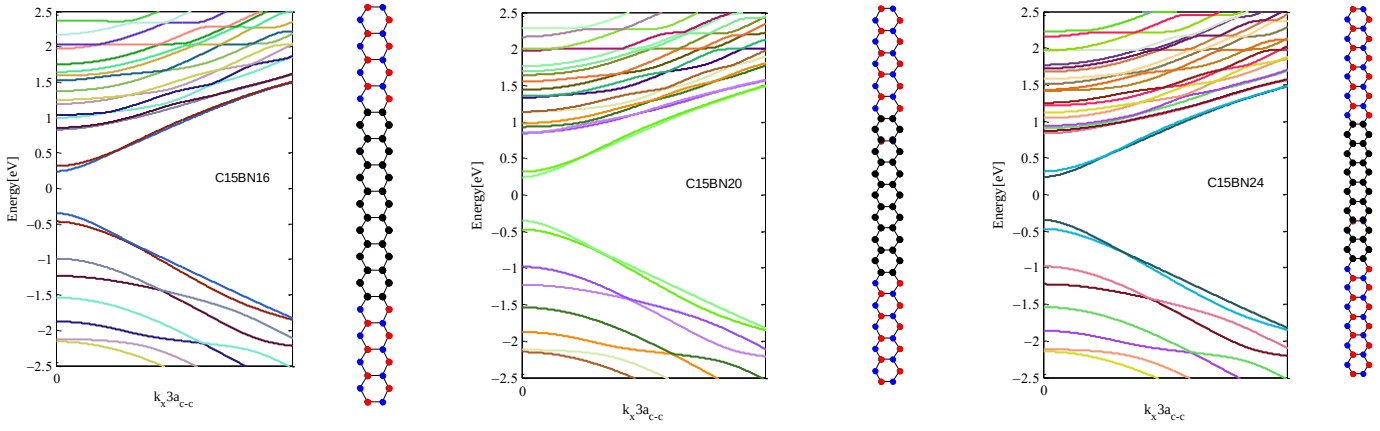
C15BN16
C15BN20
C15BN24
Energy[eV]
$k_x 3a_{c-c}$

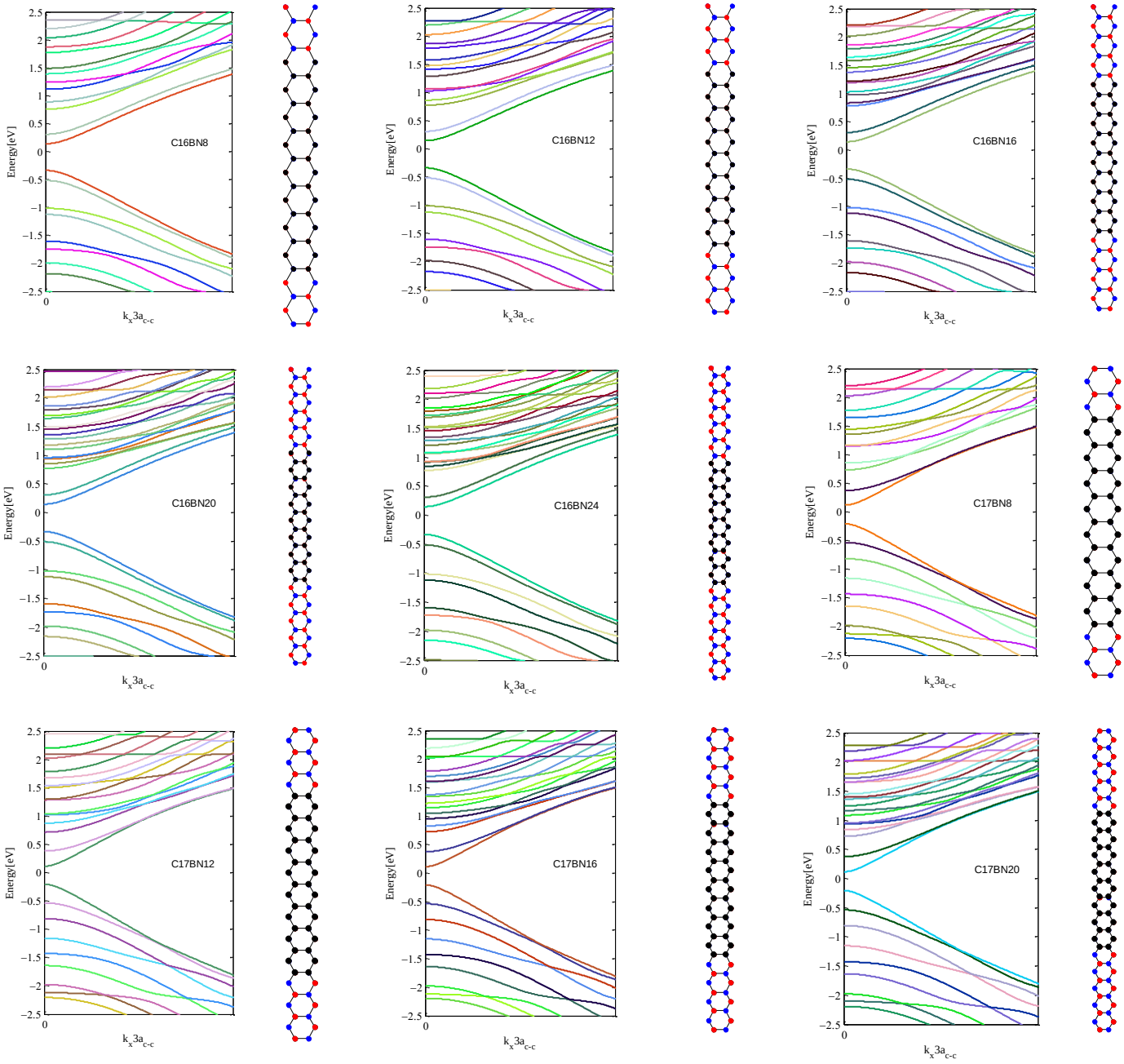
C16BN8
C16BN12
C16BN16
C16BN20
C16BN24
C17BN8
C17BN12
C17BN16
C17BN20
Energy[eV]
k_x3a_c-c

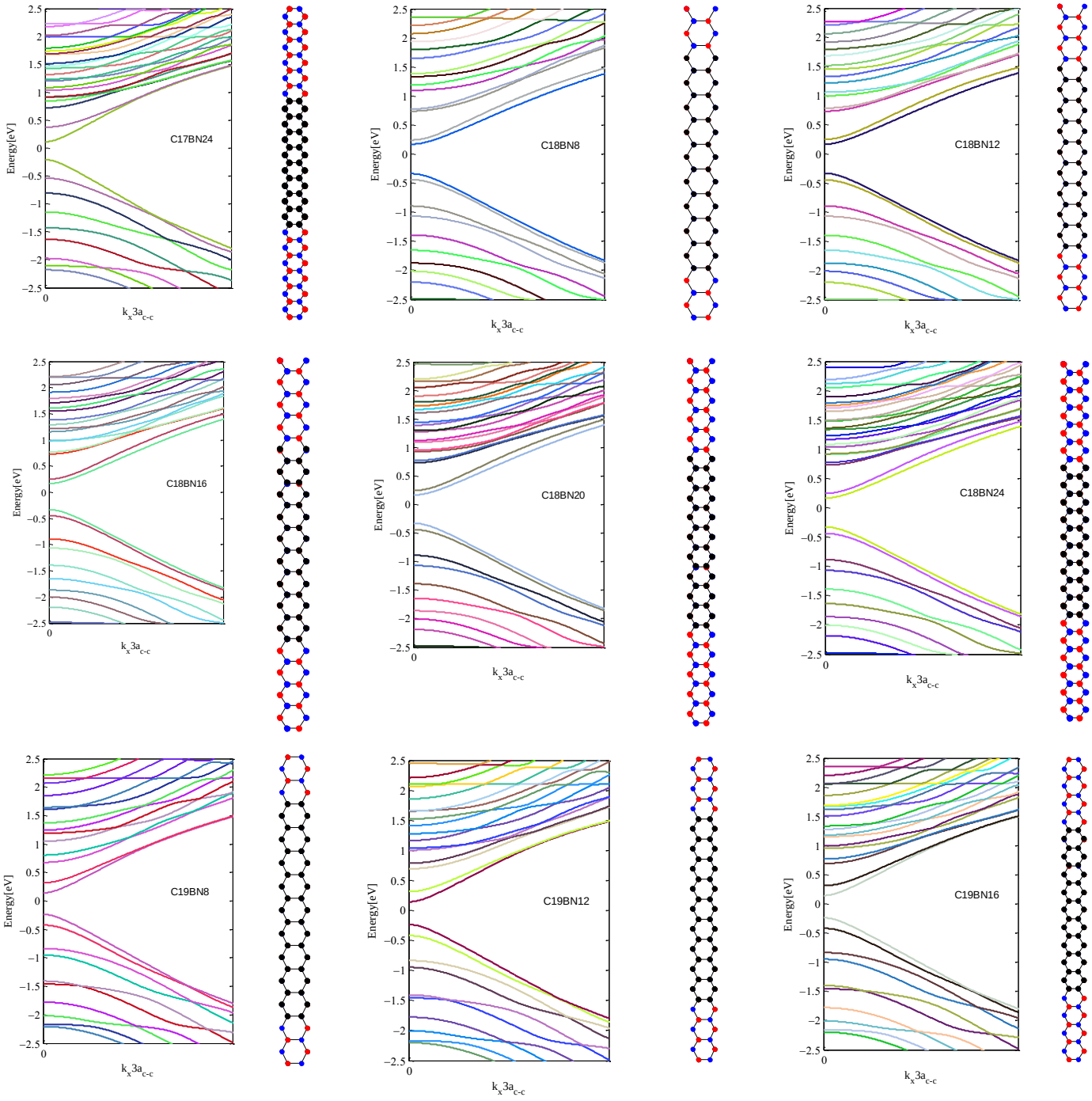
C17BN24
C18BN8
C18BN12
C18BN16
C18BN20
C18BN24
C19BN8
C19BN12
C19BN16
Energy[eV]
k_x3a_c-c

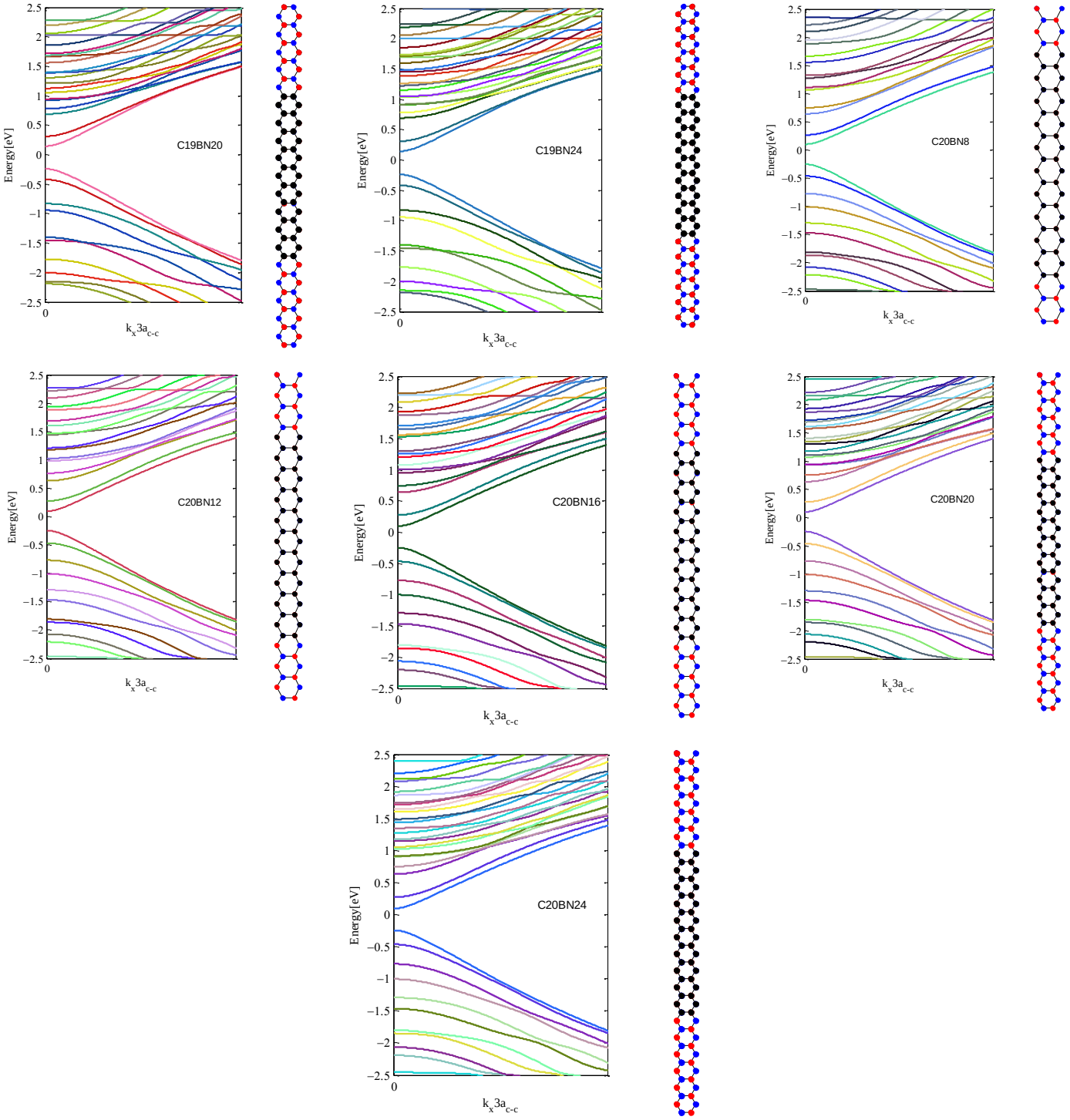

Fig.4.3.1: Bandgap Analysis of ABNNR confined AGNR

The band gaps obtained from these analyses follow a three family hierarchy of AGNR. The only difference in that, here for 3p+2 width indexes, there exists a valid bandgap. The established bandgaps are stated as follows:

Table VI
Data of Bandgap Analysis of ABNNR confined AGNR

C_xBN_y	Tight binding bandgap value (eV)	C_xBN_y	Tight binding bandgap value (eV)
C_5BN_8	0.8423	$C_{13}BN_8$	0.5205
C_5BN_{12}	0.8067	$C_{13}BN_{12}$	0.5253
C_5BN_{16}	0.5937	$C_{13}BN_{16}$	0.5283
C_5BN_{20}	0.6003	$C_{13}BN_{20}$	0.5292
C_5BN_{24}	0.6004	$C_{13}BN_{24}$	0.5251
C_6BN_8	1.2024	$C_{14}BN_8$	0.4710
C_6BN_{12}	1.1731	$C_{14}BN_{12}$	0.4629
C_6BN_{16}	1.1838	$C_{14}BN_{16}$	0.4648
C_6BN_{20}	1.2742	$C_{14}BN_{20}$	0.4604
C_6BN_{24}	1.2738	$C_{14}BN_{24}$	0.4601
C_7BN_8	0.8458	$C_{15}BN_8$	0.6632
C_7BN_{12}	0.8547	$C_{15}BN_{12}$	0.5954
CBN_{16}	0.8553	$C_{15}BN_{16}$	0.5925
C_7BN_{20}	0.8576	$C_{15}BN_{20}$	0.5965
C_7BN_{24}	0.8605	$C_{15}BN_{24}$	0.5899
C_8BN_8	0.7881	$C_{16}BN_8$	0.4792
C_8BN_{12}	0.7170	$C_{16}BN_{12}$	0.4850

C_8BN_{16}	0.7196	$C_{16}BN_{16}$	0.4810
C_8BN_{20}	0.5833	$C_{16}BN_{20}$	0.4756
C_8BN_{24}	0.6333	$C_{16}BN_{24}$	0.4775
C_9BN_8	0.9196	$C_{17}BN_8$	0.3292
C_9BN_{12}	0.8879	$C_{17}BN_{12}$	0.3201
C_9BN_{16}	0.8893	$C_{17}BN_{16}$	0.3194
C_9BN_{20}	0.8882	$C_{17}BN_{20}$	0.3209
C_9BN_{24}	0.7888	$C_{17}BN_{24}$	0.3200
$C_{10}BN_8$	0.7071	$C_{18}BN_8$	0.5129
$C_{10}BN_{12}$	0.7140	$C_{18}BN_{12}$	0.4972
$C_{10}BN_{16}$	0.7144	$C_{18}BN_{16}$	0.4988
$C_{10}BN_{20}$	0.7008	$C_{18}BN_{20}$	0.4947
$C_{11}BN_8$	0.4724	$C_{18}BN_{24}$	0.4947
$C_{11}BN_{12}$	0.4579	$C_{19}BN_8$	0.3964
$C_{11}BN_{16}$	0.4575	$C_{19}BN_{12}$	0.3795
$C_{11}BN_{20}$	0.4577	$C_{19}BN_{16}$	0.3830
$C_{11}BN_{24}$	0.4559	$C_{19}BN_{20}$	0.3820
$C_{12}BN_8$	0.7188	$C_{19}BN_{24}$	0.3800
$C_{12}BN_{12}$	0.6977	$C_{20}BN_8$	0.34837
$C_{12}BN_{16}$	0.7016	$C_{20}BN_{12}$	0.34216
$C_{12}BN_{20}$	0.6898	$C_{20}BN_{16}$	0.34236
$C_{12}BN_{24}$	0.6952	$C_{20}BN_{20}$	0.34203
$C_{13}BN_8$	0.5205	$C_{20}BN_{24}$	0.34035

Using the following data table (Table.4.3.2) we can evaluate the graphical representation of band structure by varying y for all values of x. In each case the value of x is fixed.

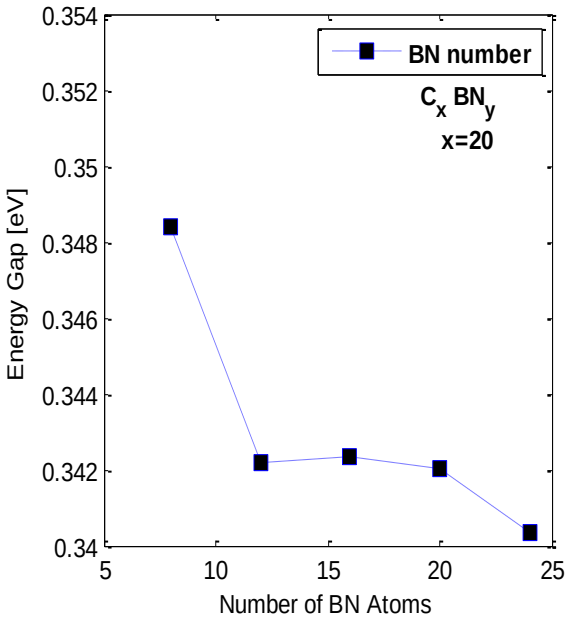

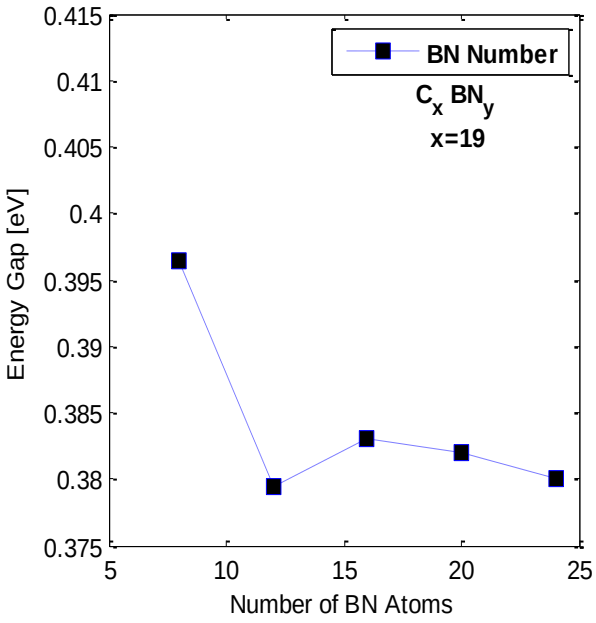

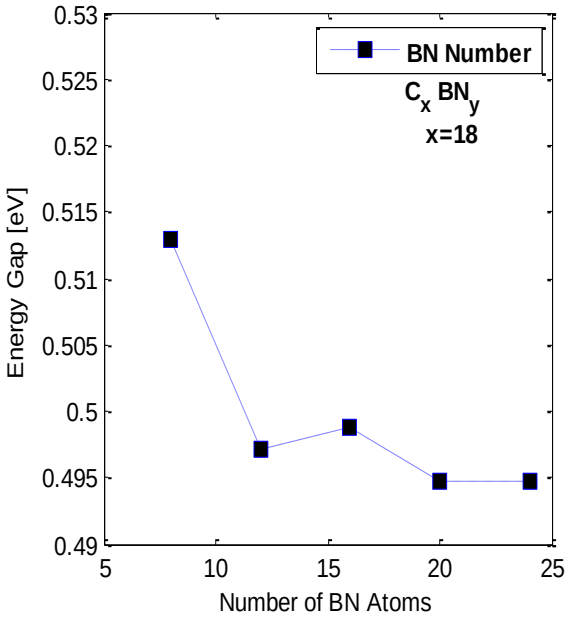

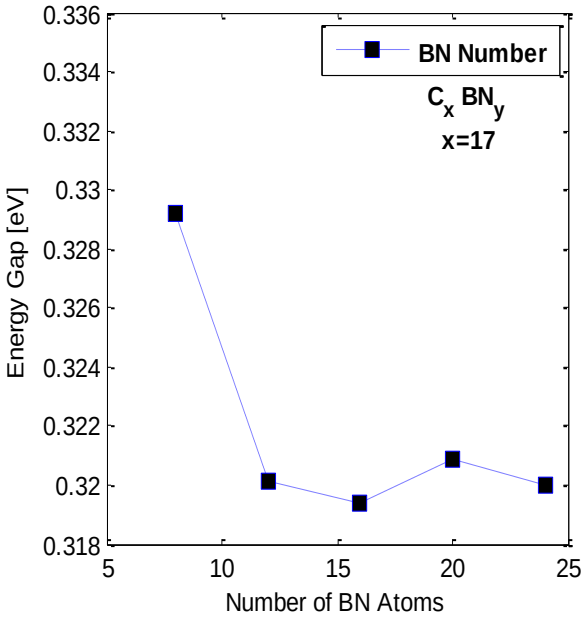

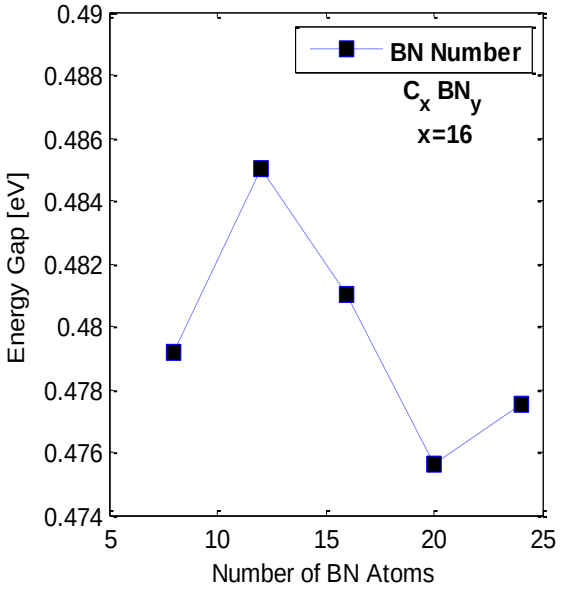
BN Number
$C_x BN_y$
x=16
Energy Gap [eV]
Number of BN Atoms
0.49
0.488
0.486
0.484
0.482
0.48
0.478
0.476
0.474
5
10
15
20
25

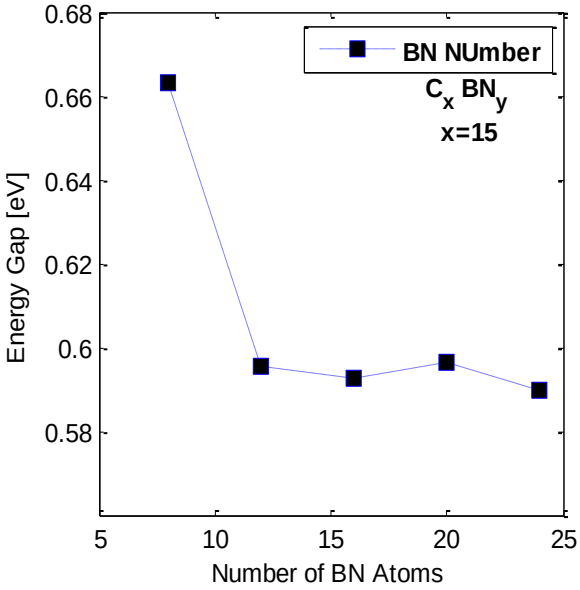
BN NUmber
$C_x BN_y$
x=15
Energy Gap [eV]
Number of BN Atoms
0.68
0.66
0.64
0.62
0.6
0.58
5
10
15
20
25

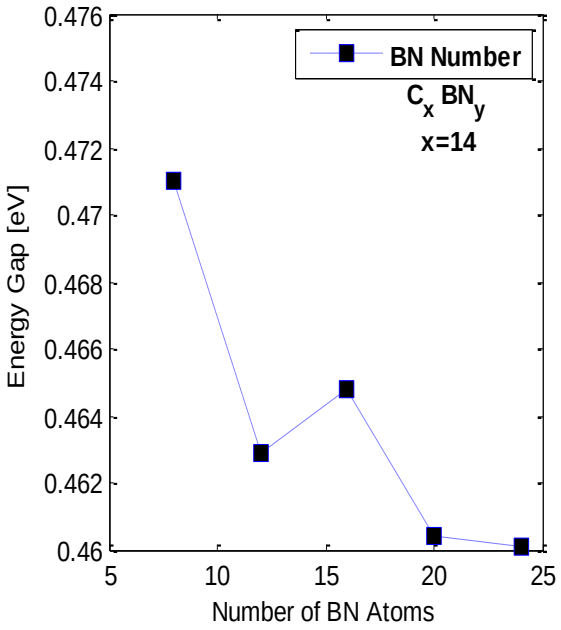
BN Number
$C_x BN_y$
x=14
Energy Gap [eV]
Number of BN Atoms
0.476
0.474
0.472
0.47
0.468
0.466
0.464
0.462
0.46
5
10
15
20
25

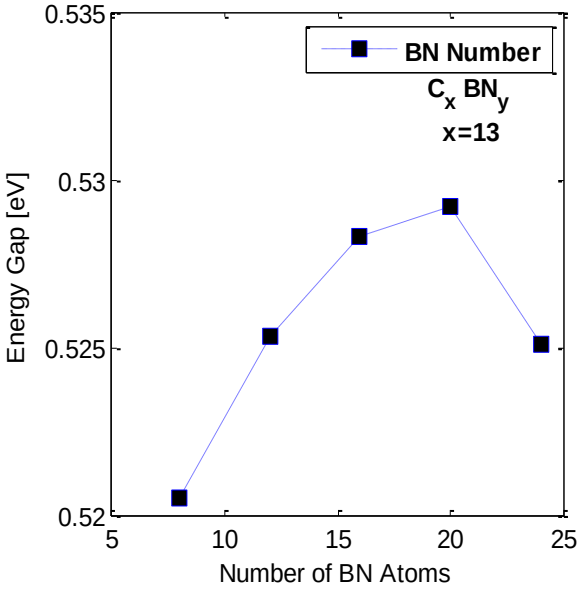
BN Number
$C_x BN_y$
x=13
Energy Gap [eV]
Number of BN Atoms
0.535
0.53
0.525
0.52
5
10
15
20
25

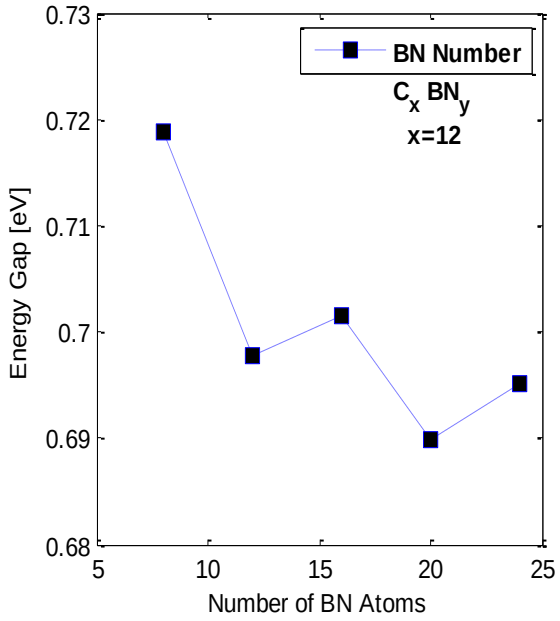
BN Number
$C_x BN_y$
x=12
Energy Gap [eV]
Number of BN Atoms
0.73
0.72
0.71
0.7
0.69
0.68
5
10
15
20
25

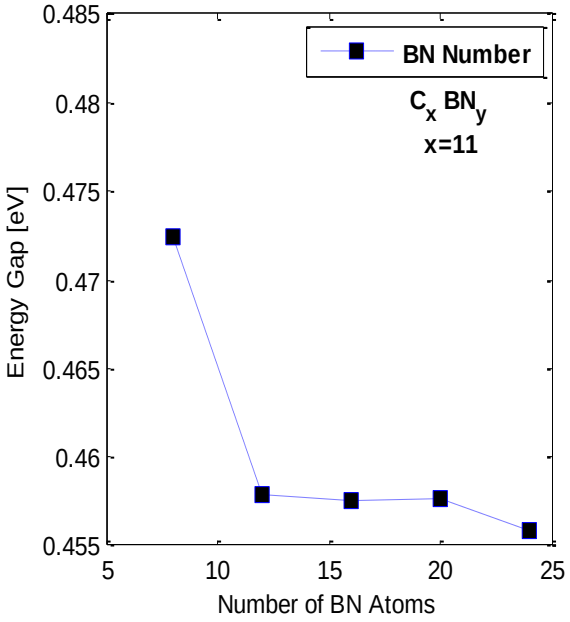
BN Number
$C_x BN_y$
x=11
Energy Gap [eV]
Number of BN Atoms
0.485
0.48
0.475
0.47
0.465
0.46
0.455
5
10
15
20
25

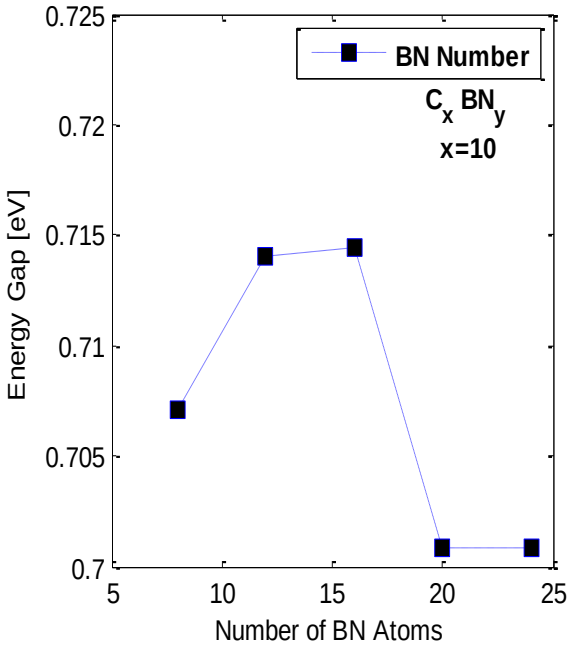
BN Number
$C_x BN_y$
x=10
Energy Gap [eV]
Number of BN Atoms
0.725
0.72
0.715
0.71
0.705
0.7
5
10
15
20
25

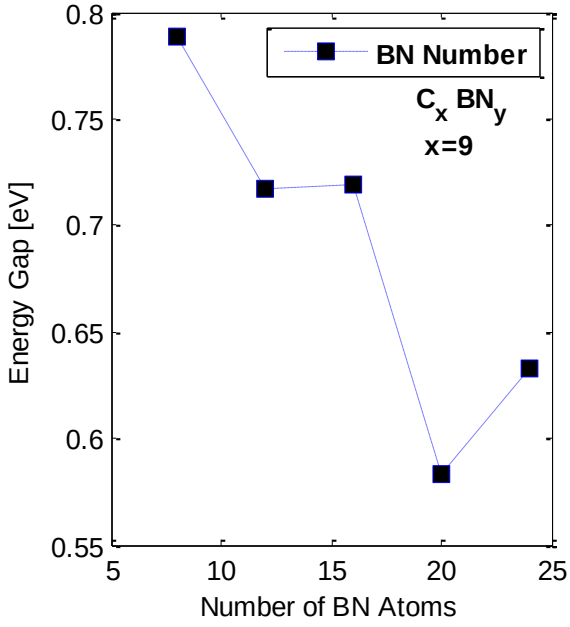
BN Number
$C_x BN_y$
x=9
Energy Gap [eV]
Number of BN Atoms
0.8
0.75
0.7
0.65
0.6
0.55
5
10
15
20
25

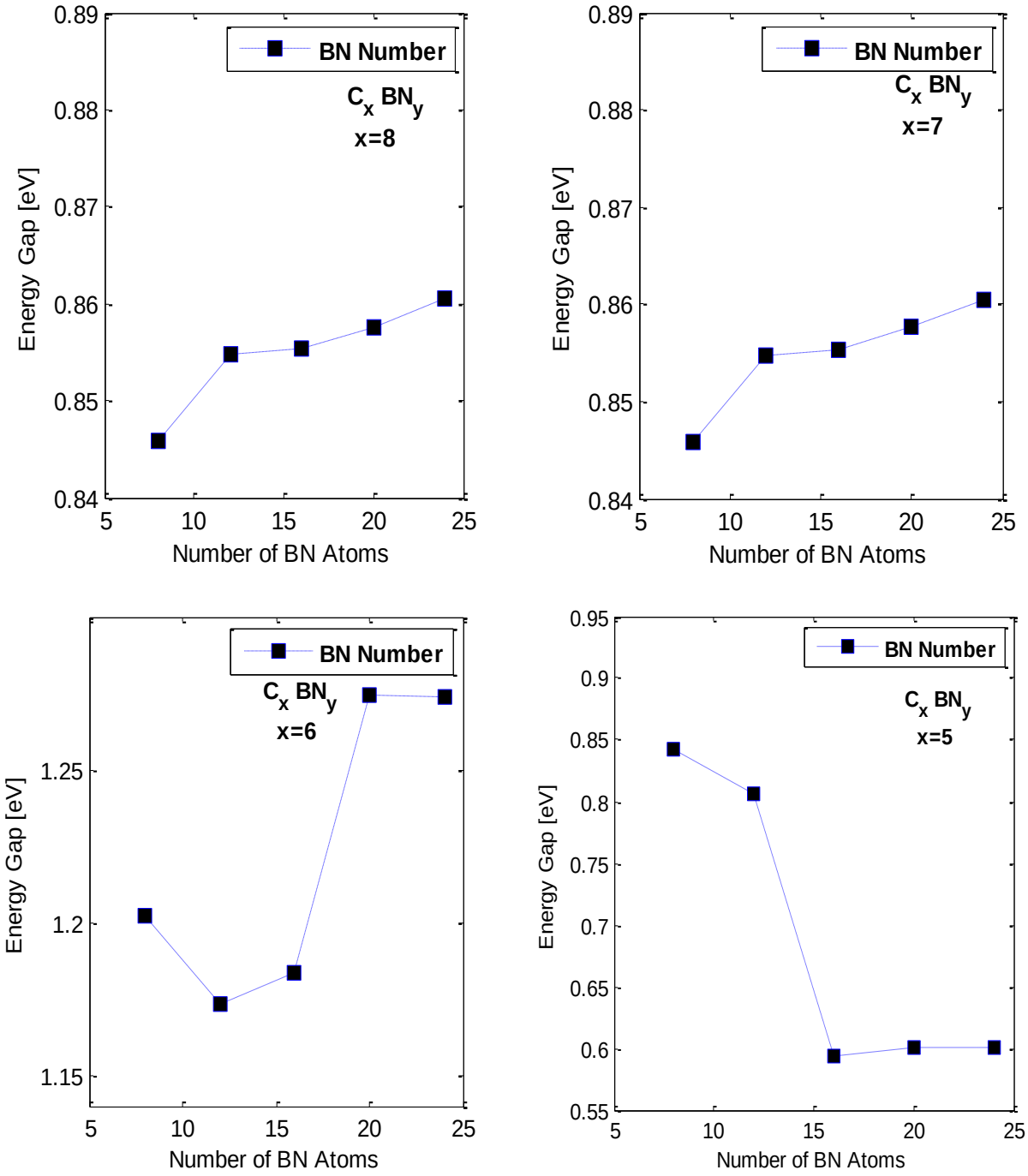

Fig 4.3.2: Graphical Representation of Bandgap of ABNNR confined AGNR For fixed number of Carbons.

Since it is evident from the analysis that A-C_xBN_y attains a stable bandgap for width index value 24 of ABNNR, a clear hierarchy relation can therefore be concluded. The following figure re-establishes the pre-claimed statement that A-C_xBN_y follows the hierarchy

of AGNNR ($E_g^{3p} > E_g^{3p+1} > E_g^{3p+2}$). The data collected for specifying the Three Family Hierarchy and the corresponding graphical representation are as follows:

Table: VII
Data Comparison for Determining Three Family Hierarchy of A-C_xBN_y

C_xBN_{24}	Tight binding bandgap value
C_5BN_{24}	0.6004
C_6BN_{24}	1.2738
C_7BN_{24}	0.8605
C_8BN_{24}	0.6333
C_9BN_{24}	0.7888
$C_{10}BN_{24}$	0.7008
$C_{11}BN_{24}$	0.4559
$C_{12}BN_{24}$	0.6952
$C_{13}BN_{24}$	0.5899
$C_{14}BN_{24}$	0.4601
$C_{15}BN_{24}$	0.5899
$C_{16}BN_{24}$	0.4775
$C_{17}BN_{24}$	0.3200
$C_{18}BN_{24}$	0.4947
$C_{19}BN_{24}$	0.3800
$C_{20}BN_{24}$	0.34035

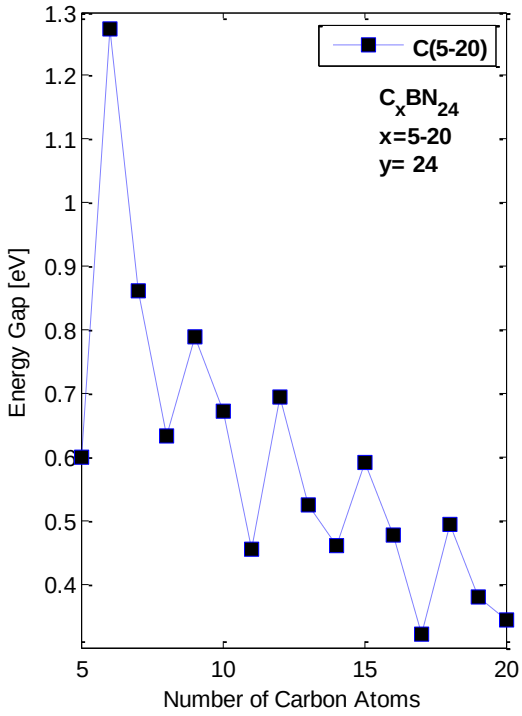

Fig. 4.3.3: Three Family Hierarchy of A-C_xBN_y

Potential combination for making Optical Devices:

Another most important conclusion that can be derived from the obtained data is that for the ribbon width index 6 of the carbon atoms stimulated bandgap is 1.2738 eV for BN's width index 24 and above. Such bandgap is useful in making optical devices. Using the electromagnetic waves equation the significance of the bandgap obtained for A-C_6BN_y (where y is 24 and above) can be evaluated. Wavelength of electromagnetic wave follows the following equation:

$$E = \frac{hc}{\lambda};$$

Where, E is the energy (bandgap) in eV, h is plank's constant, c is the velocity of light and λ is the wavelength.

Now, both plank's constant and velocity are constant terms where,

$$c = 3 * 10^8$$

$$h = 6.63 * 10^{-34}$$

Therefore,

$$\lambda = \frac{hc}{E};$$

For the ribbon width index 6 of carbon atoms $E = 1.27eV$

Thus the resultant becomes $\lambda = 9.78 * 10^{-7}$, which is suitable for optical devices according to the wavelength distribution as shown below:

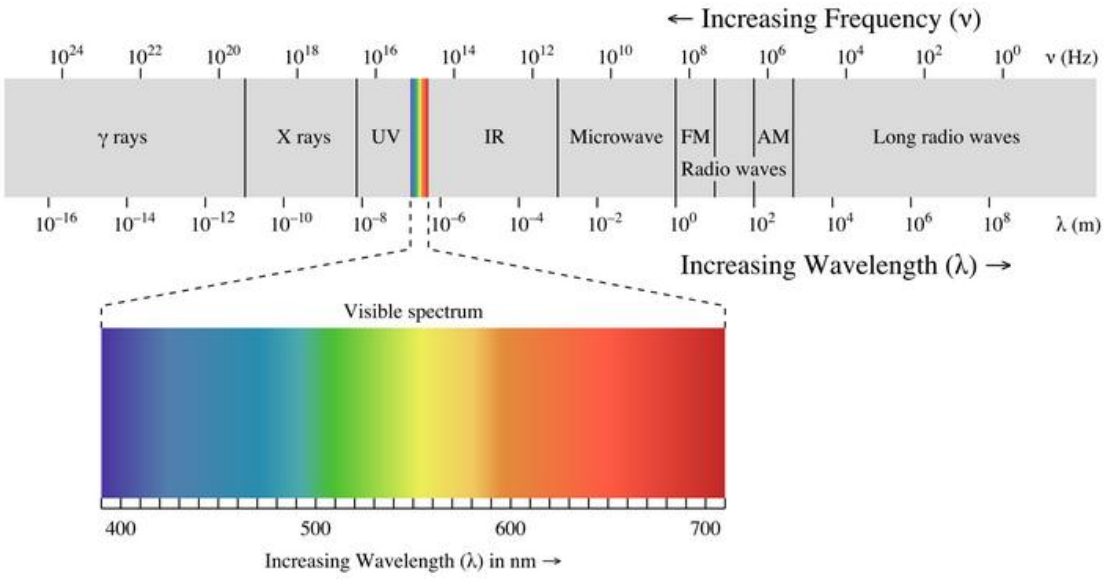

Fig. 4.3.4: Visibility spectrum. [Source: Wikipedia books (1596930284).

4.4 DOS Representation of BNNR embedded GNR:

For understanding the density of states, electron density and electrostatic difference potential a DOS evaluation using the DFT is performed. Using this representation occupied and unoccupied energy states can be evaluated.

DOS representation for BNNR embedded GNR with semiconducting width index:

(a)

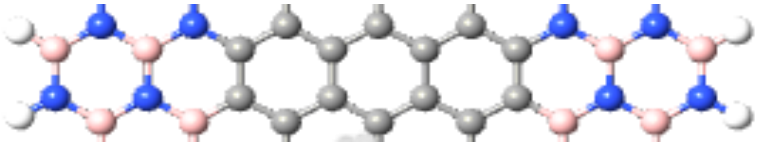

(b)

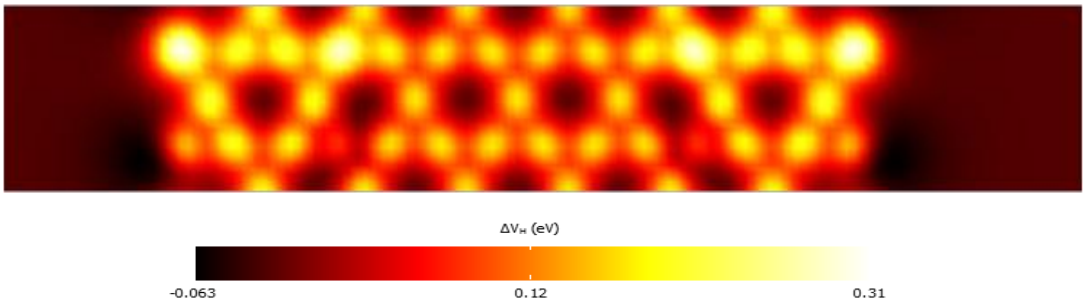

(c)

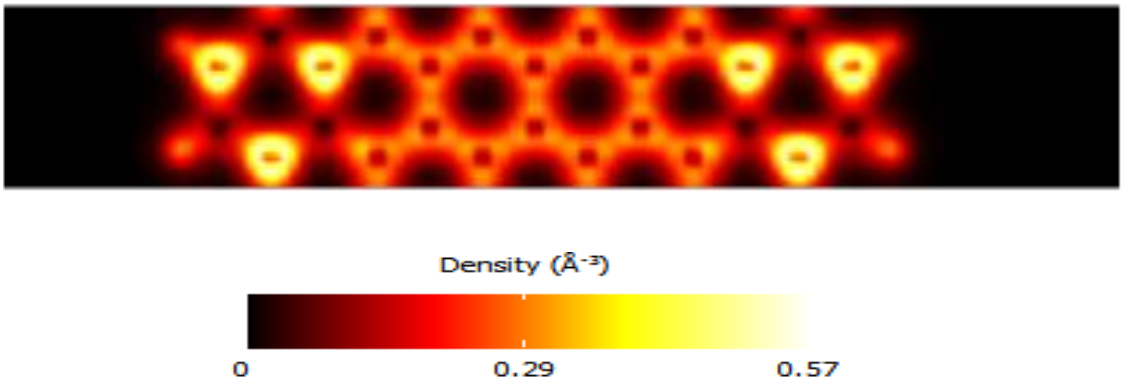

(d)

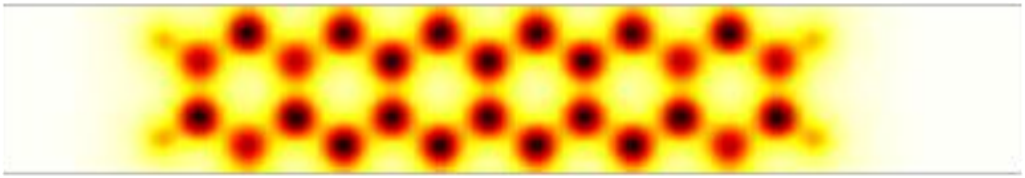

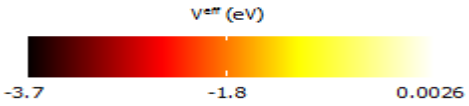

(e) (f)

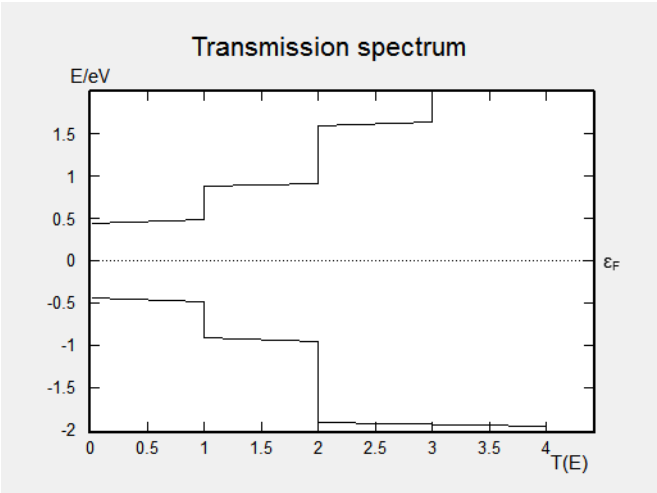

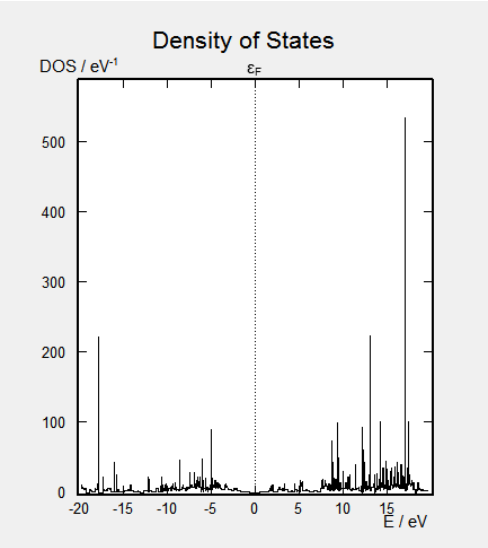

Fig. 4.4.1: (a)BNNR embedded GNR(C7BN8), (b) Electrostatic difference potential, (c) Electron density, (d) Effective potential, (e) Transmission spectrum and (f) Density of States.

Using the electrostatic difference potential the polarity of the material as well as its electrostatic force can be determined. The position of of a particular electron can be evaluated by employing electron density. Again effective potential helps to calculate the orbitals engaged in bonding and anti-bonding mechanism. Form the transmission spectrum above it can be concluded that such Nano ribbons can be used to make better nano scale semiconducting devices.

DOS representation for BNNR embedded GNR with metallic width index$_{(3p+2)}$:

(a)

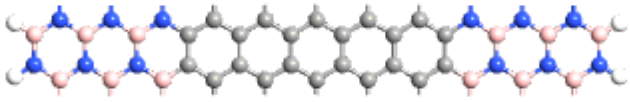

(b) (c)

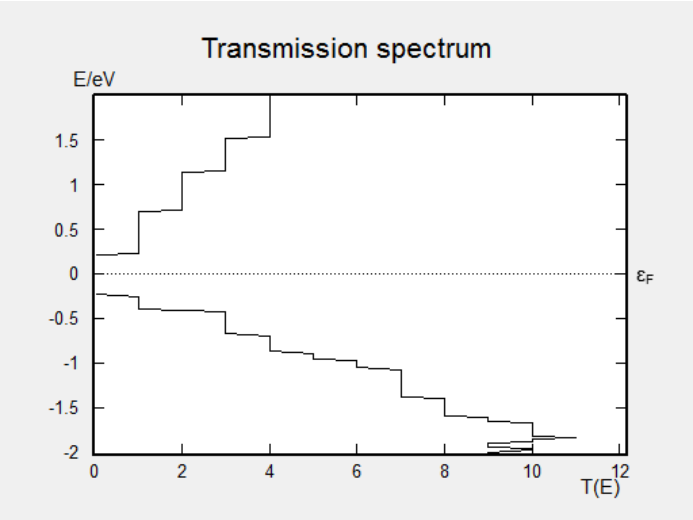

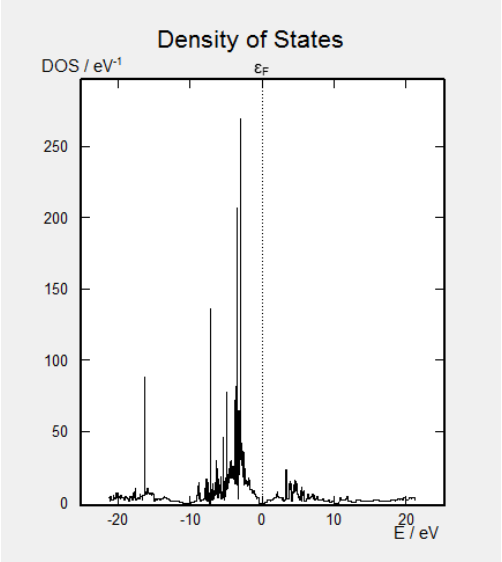

Fig. 4.4.2: (a)BNNR embedded GNR(C11BN20), (b) Transmission spectrum and (c) Density of States.

4.5 GUI Representation for finding Band Structure of AGNR and ABNNR embedded AGNR:

A Graphical User Interface (GUI) has been created based on DFT evaluated nearest TB model. The GUI enables users to calculate the band structutre of both AGNR and AGNR confined by ABNNR as well as the corresponding ribbon structures simultaneously. The execution in GUI is shown using the following figures.

(a)

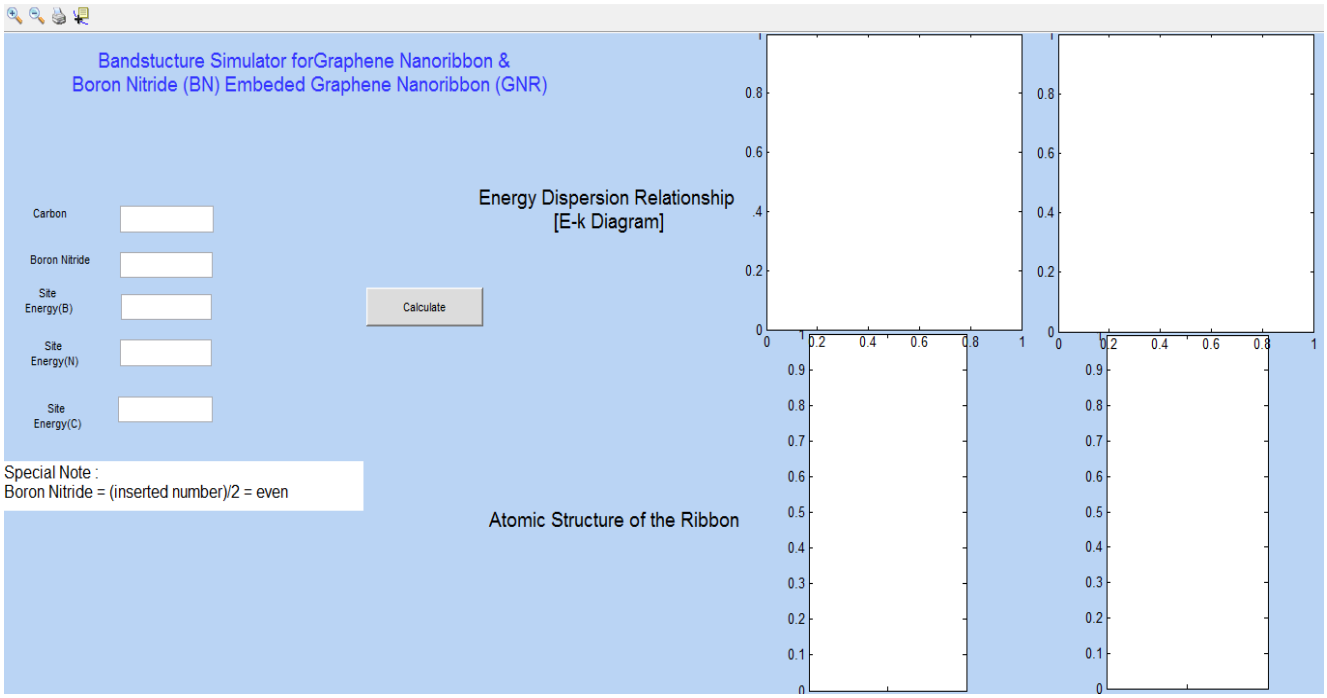
Bandstucture Simulator forGraphene Nanoribbon &
Boron Nitride (BN) Embeded Graphene Nanoribbon (GNR)
Carbon
Boron Nitride
Site Energy(B)
Site Energy(N)
Site Energy(C)
Calculate
Special Note :
Boron Nitride = (inserted number)/2 = even
Energy Dispersion Relationship
[E-k Diagram]
Atomic Structure of the Ribbon

(b)

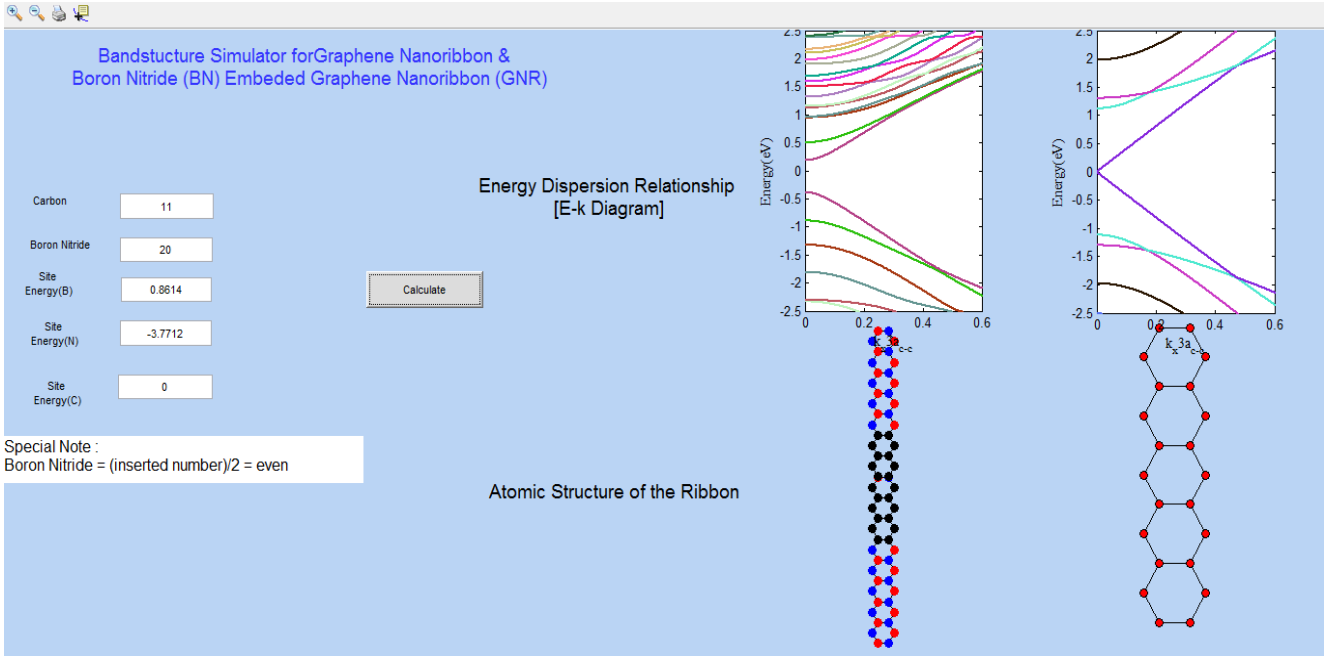

Fig. 4.5: GUI representation of band structure and ribbon of AGNR and ABNNR embedded AGNR (a) General GUI surface (b) GUI surface after calculate operation.

4.6 Summary of the Chapter:

Materials with tunable bandgap are the center of attraction for making transistors and optical devices. The fact that AGNR, when embedded in ABNNR gives tunable bandgap has been the source of motivation for this research. Therefore the following chapter has been dedicated towards observing the bandgaps as well as finding all the features that contribute to the bandgap opening.

Chapter 5: Conclusion

5.1 Summary:

The research in finding a tunable bandgap for ABNNR embedded AGNR was a success after several months of dedicated hard work. The key objective of this paper was to find out the bandgap variation for metallic width indexes, moreover, determine the most approximate parameters that enable the nearest TB model to reciprocate the resultants obtained from DFT calculation. The procedure for establishing such a TB model was based on traditional quantum physics methodologies, starting from the General Schrodinger's equation to density of states. The validity of the proposed TB model has been further illustrated by direct comparison of the output with DFT calculation.

5.2 Proposed Methods for improving bandgap:

Since the on-site energy of AGNR tends to zero, edge localization depends on on-site energies of ABNNR. In this paper, the on-site energies of ABNNR are calculated using the fermi level energy and energy gap of ABNNR. However, these values of on-site energies can be further illustrated by using the fermi level energy and energy gap of ABNNR embedded AGNR. This process has been incorporated in the paper and after due research for best adjusted parameters, the on-site energies of ABNNR have been used repeatedly along with the approximated hopping parameters. The variation of the on-site energies is likely to provide better bandgap resultants in future work.

5.3 Future Scope of Work:

Previously only graphene was used to fabricate Nano Ribbons for various device applications but analogous structure of BNNR has triggered new scientific investigation. The application of BNNR confined AGNR has not only added new dimensions in field of FETs but also encouraged possibilities of attaining suitable bandgap for optical devices. The potential bandgap also leads to enormous application is digital electronics, pseudo spintronic, terahertz technology, infrared Nano-photonics and many more high speed switching devices. Therefore fabrication of embedded AGNR in other heterostructures has the potential to open a bandgap suitable for optical devices.

Reference:

1. A. Pakdel, D. Golberg, Chem. Soc. Review, 43 (2014) 934-959.
2. M. K. Denk, Inorganic Chemistry (2000)
3. K. Zhao, M. Zhao, Z. Wang, Y. Fan, Phys. Rev. E 43 (2010) 440-445.
4. G. Seol, J. Gua, Applied Physics Letter 98, 143107 (2011).
5. M. Topsakal, E. Akturk, S. Ciraci, Phys. Rev. B 79 (2009) 115442.
6. C.H. Park, S.G. Louie, NanoLett. 8 (2008) 2200.
7. Z. Zhang, W. Guo, Phys. Rev. B 77 (2008) 075403.
8. Z.G. Chen, J. Zou, G. Liu, F. Li, Y. Wang, L. Wang, X.-L. Yuan, T. Sekiguchi, H.M. Cheng, G.Q. Lu, Am. Chem. Soc. Nano 2 (10) (2008) 2183.
9. E. Bekaroglu, M. Topsakal, S. Cahangirov, S. Ciraci, Phys. Rev. B 81 (2010) 075433.
10. Y.W. Son, M.L. Cohen, S.G. Louie, Phys. Rev. Lett. 97 (2006) 216803.
11. H. Hiura, Appl. Surf. Sci. 222 (2004) 374.
12. C. Berger, Z. Song, T. Li, X. Li, A. Y. Ogbazghi, R. Feng, Z. Dai, A.N. Marchenkov, E.H. Conrad, P.N. First, W.A. de Heer, J. Phys. Chem. B 108 (2004) 19912.
13. Y. Zhang, Y.W. Tan, H.L. Stormer, P. Kim, Nature (London) 438 (2005) 201.
14. K.S. Novoselov, A.K. Geim, S.V. Morozov, D. Jiang, M.I. Katsnelson, I.V. Grigorieva, S.V. Dubonos, A.A. Firsov, Nature (London) 438 (2005) 197.
15. J. Jung, A.H. MacDonald, Phys. Rev. B 79 (2009) 235433.
16. K. Hannewald, V.M. Stojnovic, J.M. Schellekens, P.A. Bobbert, G. Kresese, J. Hafner, Phys. Rev. B 69 (2004) 075211.
17. M. Ezawa, Phys. Rev. B73, 045432 (2006).
18. M. Y. Han, B. Őzyilmaz, Y. Zhang, and P. Kim, Phys. Rev. Lett.98 (2007) 206805.
19. F. Zheng, K. Sasaki, R. Saito, W. Duan, and B.-L. Gu, J. Phys. Soc. Jpn.
20. Z. Zhang and W. Guo, Phys. Rev. B77 (2008) 075403.

21. Y. Ding, Y. Wang, and J. Ni, Appl. Phys. Lett. 95 (2009) 123105.
22. F. Zheng, G. Zhou, Z. Liu, J. Wu, W. Duan, B.-L. Gu, and S. B. Zhang,Phys. Rev. B78 (2008) 205415.
23. Z. Wang, H. Hu, and H. Zeng, Appl. Phys. Lett. 96 (2010) 243110.
24. N. Kerszberq and P. Suryanarayana, RSC Adv., 5, (2015) 43810-43814.
25. L. Ci, L. Song, C. Jin, D. Jariwala, D. Wu, Y. Li, A. Srivastava, Z. F. Wang, K. Storr, L. Balicas, F. Liu, and P. M. Ajayan, Nature Mater,9(2010) 430.